JCB Journal of Cell Biology

ARTICLE

Cell-free formation and interactome analysis of caveolae

WooRam Jung[1], Emma Sierecki[1], Michele Bastiani[1], Ailis O'Carroll[1], Kirill Alexandrov[1], James Rae[1], Wayne Johnston[1], Dominic J.B. Hunter[1], Charles Ferguson[1], Yann Gambin[1], Nicholas Ariotti[1], and Robert G. Parton[1,2]

Caveolae have been linked to the regulation of signaling pathways in eukaryotic cells through direct interactions with caveolins. Here, we describe a cell-free system based on *Leishmania tarentolae* (*Lt*) extracts for the biogenesis of caveolae and show its use for single-molecule interaction studies. Insertion of expressed caveolin-1 (CAV1) into *Lt* membranes was analogous to that of caveolin in native membranes. Electron tomography showed that caveolins generate domains of precise size and curvature. Cell-free caveolae were used in quantitative assays to test the interaction of membrane-inserted caveolin with signaling proteins and to determine the stoichiometry of interactions. Binding of membrane-inserted CAV1 to several proposed binding partners, including endothelial nitric-oxide synthase, was negligible, but a small number of proteins, including TRAF2, interacted with CAV1 in a phosphorylation-(CAV1^{Y14})–stimulated manner. In cells subjected to oxidative stress, phosphorylated CAV1 recruited TRAF2 to the early endosome forming a novel signaling platform. These findings lead to a novel model for cellular stress signaling by CAV1.

Introduction

The eukaryotic plasma membrane is a dynamic multidomain system composed of spatially and temporally defined microdomains. Caveolae are an abundant feature of many animal cell types. These bulb-shaped invaginations are maintained and stabilized by the integral membrane protein caveolins, primarily caveolin-1 (CAV1), and by the cytoplasmic lipid-binding cavin proteins, of which PTRF/Cavin1 is essential (Parton and Simons, 2007; Hansen and Nichols, 2010; Parton and del Pozo, 2013).

In addition to the role of CAV1 in caveola formation, caveolin has been proposed to play a critical role in signal transduction. The caveolin signaling hypothesis (Lisanti et al., 1995; Couet et al., 1997b; Okamoto et al., 1998) proposed that the direct interaction of a wide range of signaling proteins with caveolins regulated their activity. The proposed binding partners included cytoplasmic signaling proteins (Src family kinases, trimeric G-protein subunits, endothelial nitric-oxide synthase [eNOS], PPAR-γ, and B-catenin; Li et al., 1995; Feron et al., 1996; García-Cardeña et al., 1996; Song et al., 1997; Mo et al., 2010; Burgermeister et al., 2011) and membrane proteins (Ras, Patched, B-adrenergic receptors [B-ARs], and adiponectin receptors; Song et al., 1996; Couet et al., 1997b; Karpen et al., 2001; Wang et al., 2012). The first observation of a scaffolding function for CAV1 was made in vitro and implicated a specific region in CAV1, amino acids 81–101, in binding to the signaling proteins (Li et al., 1995). This domain, termed the caveolin scaffolding domain (CSD), interacted with itself and also modulated the activities of signaling proteins such as heterotrimeric G-proteins, Src kinase, and H-Ras (Li et al., 1995, 1996a). Phage display screening of a peptide library with the GST-CSD fusion protein identified a group of high-affinity CSD binding peptides with the consensus sequence ϕXϕXXXXϕ, ϕXXXXϕXXϕ, or ϕXϕXXXXϕXXϕ, where ϕ is an aromatic residue (Phe, Tyr, or Trp) and X is any amino acid. This loose consensus sequence was termed the "caveolin binding motif" (CBM; Couet et al., 1997b). Many proteins contain such motifs and thus are potential binding partners with the CSD (Pike, 2005), and unsurprisingly, many of the proteins that coimmunoprecipitated with caveolin contained CBM sequences (Liu et al., 2002; Byrne et al., 2012; Collins et al., 2012).

Despite the general acceptance and abundant literature supporting this caveolin signaling hypothesis, several pivotal questions have never been systematically addressed. One major concern is the accessibility of the CBM in the proposed

[1]The University of Queensland, The Institute for Molecular Bioscience, Brisbane, Queensland, Australia; [2]The University of Queensland, The Centre for Microscopy and Microanalysis, Brisbane, Queensland, Australia.

Correspondence to Robert G. Parton: r.parton@imb.uq.edu.au; Nicholas Ariotti: n.ariotti@unsw.edu.au; Yann Gambin: y.gambin@unsw.edu.au; W. Jung's present address is Center for Cancer Research, National Cancer Institute-Frederick, Frederick, MD; N. Ariotti's present address is Electron Microscope Unit, Mark Wainwright Analytical Centre, The University of New South Wales, Sydney, New South Wales, Australia; E. Sierecki, A. O'Carroll, and Y. Gambin's present address is EMBL Australia Node for Single Molecule Sciences, School of Medical Sciences, The University of New South Wales, Sydney, New South Wales, Australia.

caveolin-binding proteins. Recent research using tertiary structural information argues that the CBMs from more than 40 caveolin-interacting proteins do not adopt a consensus structure (Collins et al., 2012). Moreover, for a large majority of cases, these residues are spatially unavailable for direct interactions. The second concern pertains to the physical availability of the CSD for CBM binding. Recent data suggest that CSD domain of CAV1 is tightly associated with the membrane and therefore unavailable for interaction with (at least) soluble proteins (Ariotti et al., 2015). Third, CBMs are not enriched in CAV1 binding proteins or conserved in species which express caveolins (Byrne et al., 2012; Collins et al., 2012). More generally, the proposed universal role for CAV1 in regulating so many signaling pathways would be expected to result in serious deleterious effects to normal cell growth and function. However, double knockout CAV1/CAV3 mice are still viable and fertile (Drab et al., 2001; Razani et al., 2001; Park et al., 2002). These contradictions, as well as the mechanistic considerations of how the association between the proposed CBMs and the caveolin scaffolding domain can be reversibly regulated in cells, have led to questions about this proposed direct interaction mechanism for CAV1 control signal transduction pathways.

The role of phosphorylation of tyrosine14 of CAV1 ($CAV1^{Y14\text{-}P}$) as a crucial feature of CAV1 signaling has not received the same level of attention in the literature compared with the role of the CSD. Originally, CAV1 was identified as a major v-Src substrate in Rous sarcoma virus–transformed chick embryo fibroblasts (Glenney and Zokas, 1989). Tyrosine-phosphorylated CAV1 is tightly regulated in cells (Mastick et al., 1995) and occurs in response to various stimuli (Scherer et al., 1994; Zhang et al., 2007; Joshi et al., 2012). Other studies have suggested the regulatory role of phosphorylated tyrosine14-CAV1 ($CAV1^{Y14\text{-}P}$) in mechanosensation (Volonté et al., 2001), signal transduction cascades (del Pozo et al., 2005; Zhang et al., 2007; Joshi et al., 2012), and endocytosis (Parton and del Pozo, 2013; Zimnicka et al., 2015). Moreover, several $CAV1^{Y14\text{-}P}$–dependent interactions with signaling proteins have been identified. These include interactions with Src family kinases and with TNF receptor–associated factor 2 (TRAF2; Wary et al., 1998; Cao et al., 2002).

We have previously suggested that the in vitro interaction of purified caveolin domains with proteins of interest may be misleading as a result of the inherent amphipathic nature of the CSD and may not represent an in vivo interaction, particularly if the CSD is embedded within the membrane of caveolae (Ariotti et al., 2015). Similarly, for detergent-insoluble proteins, such as caveolin, standard immunoprecipitation (IP) approaches may be difficult to interpret (Parton and Simons, 2007). A simplified model system for the formation of caveolae which allows systematic investigation of interacting partners would represent a major advance. Here, we present a cell-free (cf) caveola reconstitution system that uses a *Leishmania tarentolae* (*Lt*) extract (LTE) (Mureev et al., 2009; Kovtun et al., 2011). This system enables rapid expression of fluorescently labeled caveolins in vitro that leads to formation of membrane structures with the morphology of caveolae that faithfully mimic native membrane insertion of CAV1. We show that we can induce tyrosine phosphorylation on CAV1 in this system and use it to test the interaction of native and phosphorylated caveolins with the potential targets. We tested over 20 putative caveolin-binding proteins and show that few of the described interacting proteins demonstrate detectable interactions with membrane-inserted caveolin. We confirm these interactions in cells and show that $CAV1^{Y14\text{-}P}$ binds to, and recruits, TRAF2 on the cytoplasmic face of the early endosome to generate a novel signaling platform.

Results

Development of an in vitro system for rapid expression of membrane-inserted caveolin

cf protein synthesis has emerged as a potentially high-throughput platform for rapid expression of bioactive recombinant proteins (Sierecki et al., 2014). We sought to develop a system in which the interaction of caveolin with putative interacting proteins could be examined in a high-throughput format. Most importantly, we sought a system that faithfully recapitulated membrane insertion of caveolin in native caveolae. The relevance of studying the interaction of soluble caveolin with potential binding partners is unclear as a large portion of the caveolin molecule is membrane inserted, and this is required for caveolin oligomerization (Ariotti et al., 2015).

The recently developed *Lt* cf (LTE) system allows the expression of proteins directly from a cDNA with up to 100 µg/ml protein produced within 2 h (Mureev et al., 2009). We generated a series of GFP-tagged caveolin constructs, as summarized in Fig. 1 A, and expressed them in the LTE system. N-terminal tagging was found to be optimal for expression of caveolin constructs in the LTE system; a single protein product of the predicted molecular weight of the GFP-CAV1 fusion protein was produced with expression reaching a plateau after 1 h (Fig. 1 B).

Membrane-association of cf-synthesized CAV1

Because CAV1 is an integral membrane protein, we next investigated whether the expressed CAV1 was associated with membranes present in LTE. Immunogold electron microscopic detection of GFP-CAV1 and uranyl acetate staining revealed gold predominantly associated with membranous elements of 50–100 nm in diameter (Fig. 1 C). This suggests that CAV1 is inserted, either cotranslationally or posttranslationally, into endogenous membranes present in the lysate. This was further examined by density gradient centrifugation of the lysate after CAV1-expression. After 2-h expression of GFP-CAV1 or free GFP in the cf system, the lysates were incubated with the DiIC16 lipophilic dye to label membranes, applied to the bottom of a sucrose density gradient to allow floatation separation of lower density membrane fractions, and centrifuged to equilibrium (150,000 *g*, 16 h; Fig. 1 D). Expressed GFP was well separated from the peak of DiIC16 with GFP remaining in the dense fractions (fractions 26–32) and membranes partitioning in lighter fractions (16–17). In contrast, GFP-CAV1 cofractionated with the peak of the lipids in fractions 17–18. A small, but consistent, shift in the DiIC16 profile was observed when comparing lysates expressing GFP and GFP-CAV1. The fluorescence of GFP-CAV1 reproducibly aligned with the DilC16 lipid peak at fractions 17–18 (Fig. 1 E), suggesting CAV1 inserts into existing membranes in LTE and alters the lipid

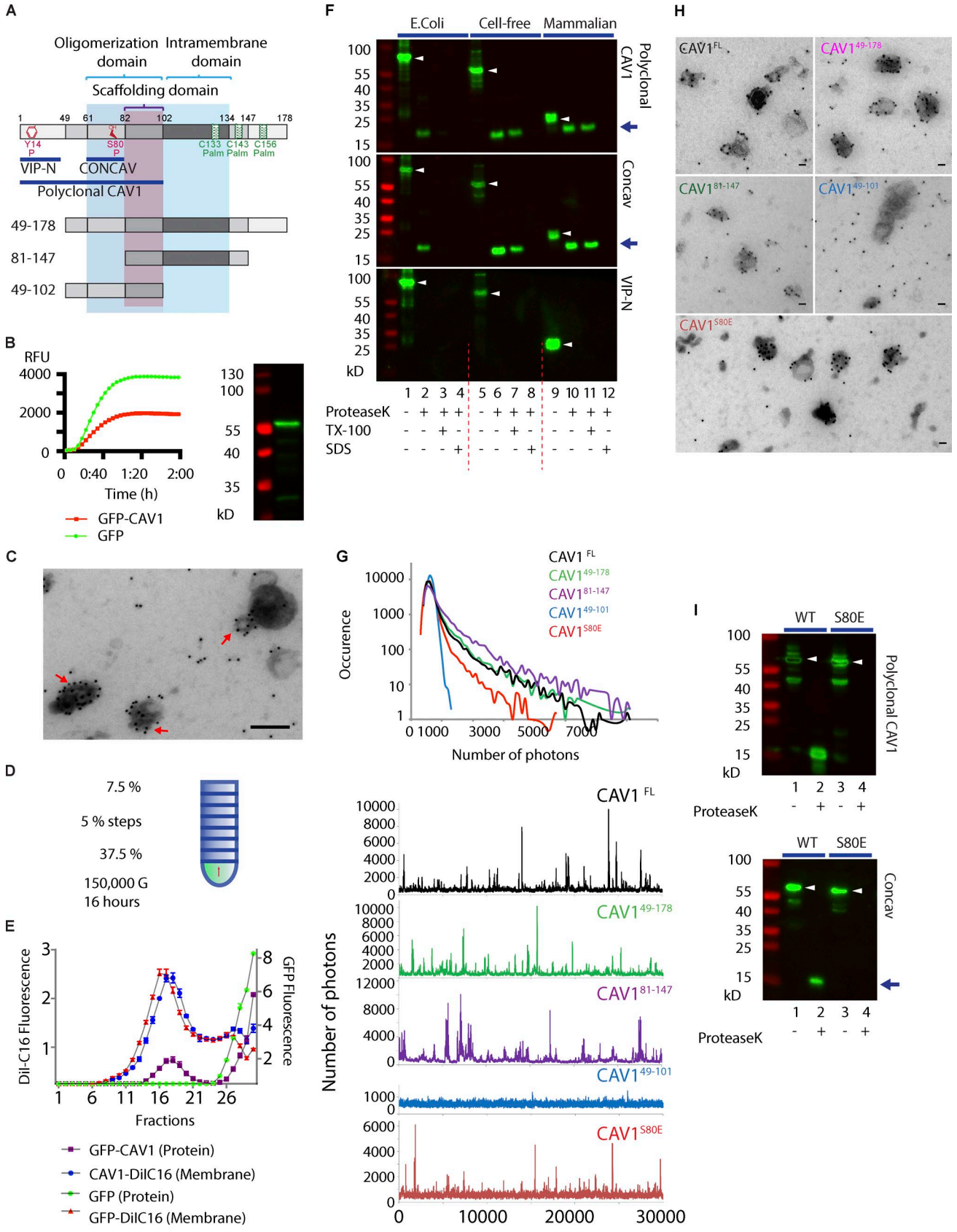

Figure 1. **Expression of caveolins in the cf LTE. (A)** Schematic representation of the sequence features of CAV1 and distinctive epitope sites on the CAV1 for the three antibodies used. VIP-N interacts with residues 1–20, Concav binds residues 67–81, and polyclonal CAV1 targets multiple residues between 1 and 97. Numbers above the line represent the amino acid number. Phosphorylation sites are indicated in red, and palmitoylation sites are shown in green. **(B)** Left: The time-trace of GFP-CAV1 production in LTE compared with GFP alone. The total yield of GFP-CAV1 is monitored by the GFP fluorescence. Right: The production

density when compared with the DilC16 profile of GFP alone. Note that this small shift was a consistent feature of GFP-CAV1 expression (Fig. 1 E shows mean ± SEM of three independent gradients). Electron microscopic analysis of the GFP-CAV1 fractions by negative staining and immunogold labeling for GFP (Fig. S1 A) showed labeling of membranous vesicles in fractions 15–20, consistent with these results, whereas LTE-synthesized GFP showed no membrane association. Intriguingly, the peak density fraction in which GFP-CAV1 sedimented (fraction 18) showed labeling of small uniform spherical structures in contrast to the more heterogeneous vesicles observed in the lighter fractions.

We next compared the in vitro membrane inserted CAV1 with endogenous CAV1 from immunoisolated mammalian caveolae and CAV1 heterologously expressed in *Escherchia coli* (*h*-caveolae; Walser et al., 2012; Ariotti et al., 2015). After synthesis of CAV1 in the cf system, membrane vesicles were separated from soluble proteins using a step gradient described as above and then treated with proteinase K (ProK), alongside purified mammalian caveolae and *h*-caveolae from *E. coli*. The resulting protein products were detected with three different caveolin antibodies that recognize different domains of CAV1 (Fig. 1 A). ProK treatment resulted in the loss of N-terminal recognition epitopes in all three model systems, indicating this region is accessible for protease-mediated degradation (Fig. 1 F). In contrast, antibodies against conserved epitopes close to the CSD recognized a protected 15-kD fragment in all three model caveola systems. This protected epitope was lost when samples were pretreated with ionic detergent (SDS) before ProK treatment. These results suggest that the membrane insertion of the cf-synthesized CAV1 mimics caveolin insertion in mammalian caveolae and other verified models of caveola biogenesis. Interestingly, protease treatment in the presence of Triton X-100 caused complete degradation of caveolin in *h*-caveolae from *E. coli*, but not CAV1 in mammalian caveolae or in *Lt*-synthesized caveolae. These data suggest that CAV1 is inserted within a detergent-resistant membrane (DRM)-like membrane environment in the *Lt* lysate, as in mammalian caveolae.

We next used single-molecule fluorescence counting methods to characterize the oligomeric state of the expressed GFP-labeled CAV1 (Fig. 1 G). Here, we measured the amplitude of fluorescent bursts reflecting individual GFP-tagged particles entering the confocal detection volume. Using the photon emission of a single GFP as a calibration factor, we could estimate the number of fluorophores present in a given particle (Sierecki et al., 2014). Full-length ($CAV1^{FL}$) GFP-CAV1 (amino acids 1–178) possessed 100–200 GFP fusion proteins per particle; this closely aligns with the number of caveolin proteins per caveola observed in a cell culture system (Pelkmans and Zerial, 2005) and in a model bacterial system (Walser et al., 2012) measured previously. Similarly, truncated constructs lacking the N terminus ($CAV1^{49–178}$) and the N and C termini ($CAV1^{81–147}$) demonstrated equivalent numbers of fluorophores per quanta. In contrast, CAV1 lacking the putative membrane-inserted hairpin domain ($CAV1^{49–101}$) behaved as a soluble protein and demonstrated loss of higher order formation. Immunogold labeling confirmed that $CAV1^{49–101}$, unlike the other CAV1 proteins tested, did not associate with membranes (Fig. 1 H) and closely resembled the profile of untagged GFP. These data suggest that the intramembrane domain of CAV1 is essential for membrane insertion and higher order formation. We next examined the role of the CSD in membrane association using a well-characterized glutamic acid substitution at Serine80 ($CAV1^{S80E}$). $CAV1^{S80E}$ showed reduced caveola formation in a bacterial expression system (Walser et al., 2012; Ariotti et al., 2015) and in mammalian cells caused CAV1 accumulation in the Golgi complex (Schlegel et al., 1999; Fielding et al., 2004; Kirkham et al., 2008), an effect linked to reduced membrane insertion of the CSD (Ariotti et al., 2015). Consistent with these results $CAV1^{S80E}$ showed reduced propensity to form the highly fluorescent particles characteristic of $CAV1^{FL}$ (Fig. 1 G) and the $CAV1^{S80E}$ point mutation disrupted the membrane association of the region adjacent to the CSD. A complete loss of the recognition epitope of the Concav antibody was observed when purified $CAV1^{S80E}$-containing membranes were subjected to ProK digestion in the absence of detergent treatment (Fig. 1 I).

of CAV1 in LTE was analyzed by Western blot for GFP-tag. **(C)** Immunogold labeling of negatively stained cf-CAV1. Red arrows highlight gold labeling–enriched membrane domains. The sample was immunolabeled with GFP nanobody conjugated to MBP, incubated with an anti-MBP antibody, and then labeled with 10 nm protein A gold (PAG) reporter. Bar, 200 nm. **(D)** Schematic representation of the gradient floatation method. The sample loaded at the bottom of the centrifuge tube was separated on a stepwise Histodenz density gradient (7.5–37.5%, Histodenz in PBS); separation was based on the buoyant density during ultracentrifugation. Gradient fractions were collected from the top of the column, and the profiles of lipids and proteins were measured by the incorporation of the fluorescent DiIC16 lipophilic dye and N-terminal GFP tag, respectively, using the Synergy 4 plate reader (excitation 485 nm and emission 520 nm for GFP and 549 nm/575 nm for DiIC16). **(E)** Comparison of protein and lipid profiles between CAV1 and GFP. GFP produced in LTE was resolved by gradient floatation fractionation demonstrating that GFP (green circles) behaves as a soluble protein remaining in the bottom fractions. However, lipids (red triangles), as resolved by fluorescent dye incorporation, did migrate into the denser fractions with a peak density at fractions 16 and 17. CAV1 produced in LTE was resolved by gradient floatation fractionation and showed that the majority of CAV1 (purple squares) peaked at fractions 17 and 18 that corresponded to the lipid peak (blue circles). The caveolin-positive lipid peak shows a small but significant shift to higher densities. Error bars indicate SEM from three independent experiments. **(F)** Comparison of membrane insertion between MDCK cell-purified caveolae, heterologous caveolae purified from *E. coli* and cf-synthesized CAV1 (cf-CAV1) by protease protection assay. The samples were digested with proteinase K in the presence or absence of 0.5% Triton X-100 or 0.1% SDS and subsequently analyzed by Western blotting using conformational antibodies as indicated. White arrowheads show the full-length CAV1, and blue arrows show CAV1 after ProK digestion. **(G)** CAV1 domains required for higher order oligomer formation analyzed by single-molecule brightness experiment. Distribution of burst brightness from CAV1 and CAV1 truncation mutants produced in LTE shows deletion of the intramembrane domain (102–134) resulted in a loss of higher-order particle formation. **(H)** Immunolabeled LTE expressing $CAV1^{FL}$, $CAV1^{81–147}$, $CAV1^{49–178}$, $CAV1^{49–101}$, and $CAV1^{S80E}$. Bars, 100 nm. **(I)** Serine80 is crucial for CAV1 membrane insertion of CSD. ProK digestion of phosphomimetic mutant of Serin80 ($CAV1^{S80E}$) results in a greater digestion of cf-CAV1 recognition domain. White arrowheads show the full-length CAV1 and blue arrows show CAV1 after ProK digestion.

Overall, these results show that cf-expressed caveolin inserts into the endogenous DRM-like membranes of the LTE, and the insertion of CAV1 is similar to that of native caveolin in mammalian systems. Charged residues within the CSD renders the CAV1-CSD accessible to proteases and inhibits caveola formation.

3D ultrastructural analysis of cf caveolae; CAV1-induces membrane curvature

Electron microscopy of the peak gradient fractions showed CAV1 association with fairly heterogeneous membranous structures of 50–100 nm, but in the heavier fractions, induced by GFP-CAV1 expression (Fig. 2 A), we observed a particularly striking association with uniform 50-nm vesicles. We reasoned that such vesicles may be generated from existing membrane structures in the lysate by caveolin expression. Conventional transmission EM allows only a projection view of the stained fraction, so to gain high-resolution 3D information on the domains labeled for GFP-CAV1, we analyzed the immunolabeled, negatively stained grids by electron tomography (Fig. 2 B). The 3D information and higher resolution of this technique revealed that CAV1-directed gold particles exclusively labeled structures with highly consistent curvature, some of which were free vesicles (diameter 44 ± 1.95 nm), whereas others were connected to larger structures resembling the bulb-to-neck-to-lamella transition of a mature plasma membrane–associated caveola. Visualization of the CAV1 protein by electron tomography was facilitated by the electron density of the caveolin–antibody complexes giving a coat-like appearance. This revealed that dense labeling for the CAV1 fusion protein was only associated with areas of highly uniform curvature. Although our single molecule analyzes gave a range of distributions for the number of GFP-tagged CAV1 fusion proteins per vesicle (Fig. 1 G), this is likely a consequence of the mixed measure of larger membranes and small vesicles. Indeed, when we tested the ratio of membrane to CAV1 in the large assemblies, we found a fairly uniform distribution (Fig. S2, E and F). In contrast, these high-resolution tomographic analyses demonstrate the remarkable consistency of CAV1-induced curvature in the LTE and clearly showed the connectivity between the highly curved CAV1 domain and domain lacking CAV1 enrichment. A schematic for the insertion of CAV1 protein into the LTE membrane is depicted in Fig. 2 C. These data indicate that cf caveolae are structurally consistent, morphologically to similar to caveolae from mammalian cells, and represent a novel system to analyze high-throughput caveola interactions. Moreover, these analyses demonstrate the remarkable consistency of CAV1-induced curvature in the cf system, clearly indicate the connectivity between the highly curved CAV1 domain and domain lacking CAV1 enrichment, and show that this cf system accurately recapitulates CAV1 membrane insertion and microdomain formation observed in the cellular environment.

To further characterize the validity of this system for the analysis of CAV1-induced membrane curvature we assayed caveola formation by caveolins from different species. We have previously shown that vertebrate caveolins (from mammals, zebrafish *Danio rerio*) and an invertebrate caveolin (from the honeybee *Apis mellifera*) can generate caveolae when expressed in CAV1$^{-/-}$ cells (Kirkham et al., 2008). However, caveolin from *Caenorhabditis elegans* could not generate structures with the morphology of caveolae (Kirkham et al., 2008). By high-resolution electron tomography, caveola-like structures were induced upon expression of mammalian caveolins and invertebrate caveolin from the honey bee, *A. mellifera* (Fig. S1 B) but not with *C. elegans* caveolin, which only induced tubular/cisternal elements. This shows that there is excellent correlation of caveola formation in the in vitro system with caveola induction in other native systems (Kirkham et al., 2008).

Interaction screen design: Membrane-inserted CAV1 and CAV1$^{Y14\text{-}p}$

Caveolin has been reported to regulate several signaling proteins via a direct interaction between its CSD region (amino acids 81–101) and the proposed conserved CBM sequence of the putative interacting proteins. This direct protein–protein interaction should be readily observable in this cf system if the binding domains in the caveolin and target are accessible. Phosphorylation of the conserved tyrosine residue at position 14 (CAV1^{Y14}) located within a separate region of CAV1 has been proposed as a crucial regulatory step in signal transduction cascades (del Pozo et al., 2005; Zhang et al., 2007). We sought to establish an in vitro assay to investigate the interaction with both native membrane–associated unmodified CAV1 and CAV1$^{Y14\text{-}p}$.

Upon expression of CAV1^{FL} in the cf system, we observed formation of fully assembled caveolae, but we also detected a population of CAV1 forming much smaller assemblies or appearing soluble. This can be seen in Fig. 1 G, where the background of monomer contributes to the mean of fluorescence detected between the large fluorescent bursts. This is presumably because endogenous membranes within the lysate can be limiting, and free lipids or smaller lipid micelles would be present. The hydrophobic domain of CAV1 could be shielded by these lipidic moieties, making CAV1 soluble in cf without incorporation into flat membranes. This is important, because interpretation of the binding experiments needs to establish if the binding occurs from nonmembrane inserted or to oligomerized membrane-inserted CAV1 within the cf caveolae. This fraction of noninserted CAV1 likely mimics CAV1 proteins that would be solubilized by detergents used in proteomics experiments.

Two techniques were used to address this fundamental question: two-color single-molecule "coincidence" method and a nanobead-based protein binding assay (Amplified Luminescent Proximity Homogeneous Assay screen, or AlphaScreen). The two methods are complementary as the single-molecule fluorescence enables direct visualization of the binding of proteins to the fully assembled caveolins, whereas the AlphaScreen binding assay represents the binding of proteins at the monomer level (Fig. S2 A).

The principle of two-color single-molecule coincidence detection is schematized in Fig. 3 A. To detect binding of putative interacting proteins on caveolae, the CAV1 proteins were tagged with mCherry, and the putative interacting proteins listed in Table 1 were tagged with GFP at the N terminus. Caveolae were detected in the acquisition channel using a 561-nm laser. At the same time and in the same confocal volume, we focused a 488-nm laser to excite GFP. The fluorescence of GFP was recorded on a separate

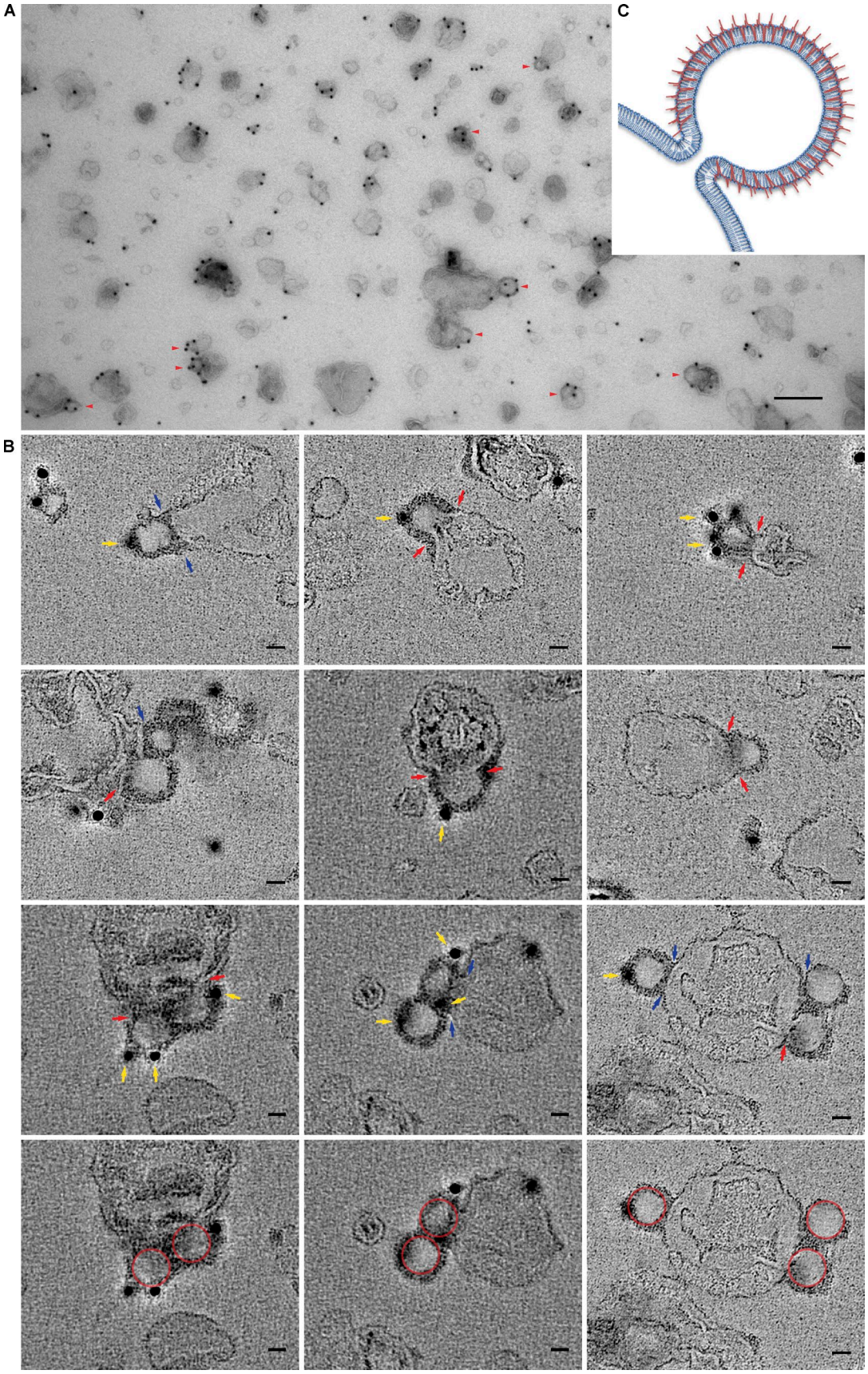

Figure 2. **Characterization of purified cf-CAV1–positive vesicles. (A)** Immuno-EM of the cf-CAV1 peak fraction showing abundant and specific cf-caveolin–positive vesicles undergoing fission from the LTE membrane (red arrowheads). Bars, 100 nm. **(B)** 3D characterization of membrane curvature generated by cf-CAV1. An optical slice from a reconstituted tomogram demonstrated the expression of CAV1 in LTE induces the formation of membrane curvature with

channel to observe the behavior of the binding partners. If a GFP-tagged protein binds to the caveolae, we detect coincident bursts of fluorescence in the GFP and mCherry channels. Fig. 3 depicts several examples from the interaction screen. The individual single-molecule time trace, from Fyn and c-Src (Fig. 3, B and C), demonstrated predominant fluorescence coincidence peaks from both channels. This reflects codiffusion of both proteins in a large complex. On the contrary, the constant, nonfluctuating fluorescence signal detected for eNOS in the presence of CAV1 oligomers indicates no measurable interaction between these proteins (Fig. 3 D).

The comparison of the GFP and mCherry intensities recorded for each peak gives a direct measure of the stoichiometry of the interaction. This ratiometric measurement has the advantage of being independent of the trajectory of the caveolae in the focal volume. As shown in Fig. 3, we can plot the histograms of stoichiometries to quantify the interactions. The Gaussian peak between 0.25 and 0.75 reflects the codiffusion of GFP and mCherry-tagged proteins. The centered peak on 0.5 from c-Src indicates 1:1 ratio interactions with CAV1, and the centered peak on 0.75 from c-Src and Fyn indicates fewer molecules in complex with CAV1. As can be seen for eNOS, the coincidence peaks on 1 indicate no interactions between two proteins (Fig. 3 D).

Overall, we tested more than 20 putative interactors identified in the literature as proteins proposed to bind CAV1 through association with phosphotyrosine14 via the CSD or proposed binding candidates with undefined interaction sites (Table 1). Only a limited number of the candidates showed significant binding to caveolae. We could detect no significant binding of the assembled caveolae to eNOS, PPAR-γ, and several other reported binding partners (Fig. 4 C). However, we observed a significant interaction with c-Src, Dynamin-2 (DNM2), Fyn, and TRAF2 with between 5 and 50 interacting molecules per caveolae, assuming that all caveolae contain ∼150 CAV1 molecules. Importantly, we have tested that these proteins do not bind to the membranes present in the cf system (see Fig. S2, J–M, for c-Src, Fyn, and eNOS compared with a GFP control).

We performed additional control experiments to validate our results, with main focus on eNOS. The fact that eNOS shows high binding affinity to other positive binding partners such as calmodulin1 (CALM1; Michel et al., 1997) indicates native folding of eNOS in the LTE (Fig. S2, B and C). We also tested $CAV1^{S80E}$, as this mutant causes the CSD to become accessible to protease digestion (Fig. 1 A; Ariotti et al., 2015) and so could allow interaction between the CSD and eNOS to be uncovered (Fig. 1 I). However, $CAV1^{S80E}$ also did not show significant interaction with eNOS (Fig. 3 E). We have also tested the short CBM sequence of eNOS (eNOS CBM [N, N terminally labeled] or [C, C terminally labeled]) that does not show any detectable binding (Fig. 4 C). The results suggest that simple protein–protein interactions between the CSD of caveolins and the CBM of diverse proteins are not involved in recruiting these signaling molecules to caveolae. In this respect, it is important to note that in vitro synthesized CAV1 showed insignificant recruitment of Cavin1 in the LTE (Fig. S3 G; note the infrequent association of CAV1 and cavin oligomers). This may be explained by the role of the lipid environment of caveolae in facilitating cavin coat recruitment (Kovtun et al., 2015). This is also an important caveat when interpreting the interaction analyses.

We next used AlphaScreen to measure binding for nonmembrane inserted or soluble CAV1. This does not represent the physiological situation with CAV1 inserted in the membrane, but may explain previous results observed by other groups using techniques that cannot differentiate between inserted and noninserted CAV1. Here, we aimed to test if the CSD domain itself can bind to different proteins. In AlphaScreen, "donor" nanobeads are functionalized with an anti-GFP nanobody, and "acceptor" nanobeads will capture the mCherry-tag (Sierecki et al., 2014). Upon binding to the mCherry-tagged CAV proteins, the positive binding partners will bring the "donor" and "acceptor" beads into close proximity. Upon excitation with a 680-nm laser, the donor beads release singlet oxygen, and the acceptor beads in immediate proximity (<200 nm) will luminesce. We coexpressed the same candidate proteins with full length CAV1 and used the noninserted $CAV1^{49\text{-}101}$ construct as a control for noninserted CAV1 (Fig. 1, G and H). We observed that a majority of the binding partners showed some interaction with nonmembrane-inserted $CAV1^{49–101}$, but the binding is even stronger for the noninserted construct (Fig. S3 B). This shows that most of the putative binding partners are capable of binding to the 49–101 domain in isolation, indicating the unusual nature of solubilized CSD peptide ($CAV1^{49–101}$). We believe that losing membrane association of CSD peptide as a result of the deletion of IMD increases the nonspecific binding of binding partners, suggesting that the membrane topology of caveolins should be considered when evaluating their interactions. This result emphasizes that the interaction analysis of CSD with CBM using the solubilized truncation mutant CAV1 cannot represent the native interactions of CAV1.

We noted that all proteins binding to the assembled caveolae are also binding at the oligomer level in AlphaScreen. For these proteins, the AlphaScreen signal displayed an unusual signature (explained in Supplemental materials; see Fig. S2 A). Overall, both used techniques showed that only c-Src, DNM2, Fyn, and TRAF2 are actually binding to the in vitro assembled caveolae.

We next tested the effect of CAV1 phosphorylation on Y14 which occurs in response to several stimuli in vivo (Mastick et al., 1995; Lee et al., 2000; Radel and Rizzo, 2005). The sequence around $CAV1^{Y14}$ is consistent with the known ABL1 substrate recognition site, YXXP (Songyang and Cantley, 1995; Li et al., 1996b), and phosphorylation of $CAV1^{Y14}$ by ABL1 has been observed in cells (Sanguinetti and Mastick, 2003) and in vitro (Mastick et al., 2001). We first investigated whether we can phosphorylate

abundant protein coat. Red arrows highlight the region of high negative curvature that resembles the neck subdomain of a mammalian caveolae between the host membrane and CAV1-enriched bulb-like domain. Blue arrows indicate the budded caveola-like vesicles. Yellow arrows represent the 10 nm gold labeling. Red circles highlight CAV1-induced curvatures. Bars, 30 nm. **(C)** Schematic representation of the caveola-like membrane curvature. The CAV1-enriched vesicle undergoes budding process by the CAV1 homooligomerization (in red).

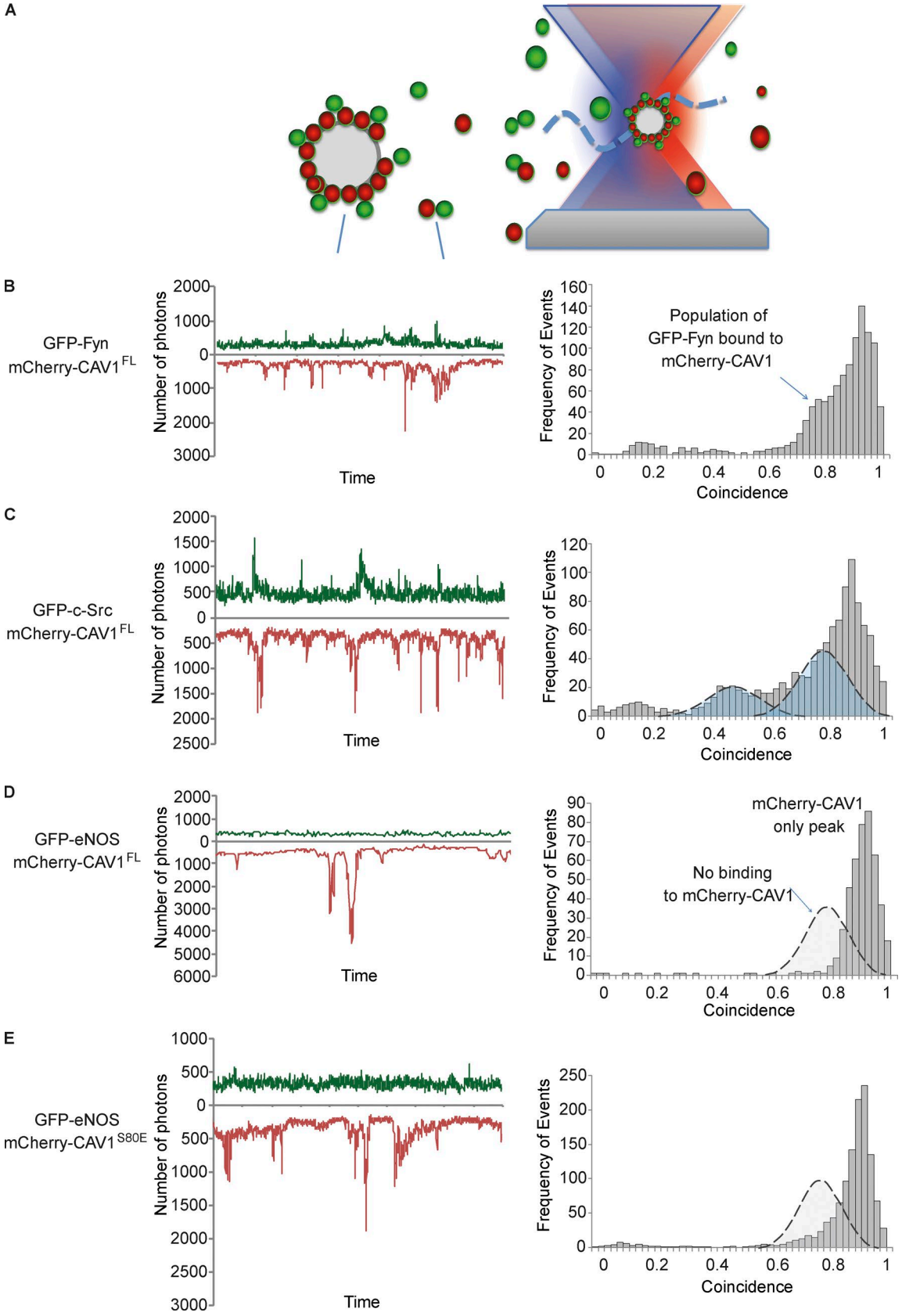

Figure 3. **Single-molecule spectroscopy allows assessing the stoichiometry of caveolae binding proteins. (A)** Schematic representation of single-molecule coincidence analysis. The use of overlapped lasers (488 nm and 561 nm) allows assessing the stoichiometry of protein heterocomplexes labeled with GFP and mCherry, respectively. **(B–E)** Individual single-molecule time trace (left) and histogram (right) for single-molecule coincidence experiments. **(B)** Fyn and CAV1 interact. Left: Codiffusion of GFP-Fyn and mCherry-CAV1 shown in coincidence peaks. Right: The Gaussian peak on 0.75 indicated with a dash curve shows the

CAV1 by coexpression with ABL1 in the cf system. When coexpressed with ABL1, cf CAV1 was phosphorylated as defined by immunoblotting with antibodies specific to $CAV1^{Y14\text{-}p}$ (Fig. S4 A). By optimization of the coexpression conditions the percentage of $CAV1^{Y14\text{-}p}$ approached ∼60% (Fig. S4, C and D), making it a suitable tool for detecting the interacting partners.

To investigate interactions with $CAV1^{Y14\text{-}p}$, we triply coexpressed mCherry-CAV1, the putative GFP-tagged interacting protein, and untagged ABL1. Phosphorylation of $CAV1^{Y14}$ increased the binding affinity of interacting partners (Fig. 4 C). Interestingly, $CAV1^{Y14\text{-}p}$ significantly increased the binding affinity of TRAF2 changing the stoichiometry from 0.75 to 0.6, resulting in an increase of binding to >100 TRAF2 per caveolae (Fig. 4, A and B). Phosphorylation also changed the overall binding affinity, as observed by AlphaScreen (Fig. S3 F). These results suggest that in this model system, CAV1 can interact with TRAF2 and that this interaction is further enhanced by phosphorylation. We tested two other members of the TRAF family. As shown in Fig. S4 G, TRAF1 and TRAF4 do not bind CAV1, even in the presence of ABL1, further confirming the specificity of the CAV1–TRAF2 interaction.

Intracellular interaction analyses; phosphorylated CAV1 associates with TRAF2 on early endosomes

To confirm the biological relevance of the observed in vitro interactions, we performed a preliminary characterization of a selection of putative CAV1-binding partners using the proximity ligation assay (PLA) in cells. HeLa cells were transfected with the GFP-labeled target protein and then analyzed by PLA using antibodies directed against GFP and endogenous CAV1. Soluble GFP, used as a negative control, produced a negligible PLA signal with endogenous CAV1, whereas Cavin1-GFP, a structural protein of caveolae (Hill et al., 2008), showed a strong signal (Fig. 5 A). In agreement with our in vitro data, eNOS and RhoA showed negligible PLA signals with CAV1. In contrast, DNM2, c-Src, TRAF2, and Fyn produced strong PLA signals with CAV1, approaching the levels obtained with the Cavin1-positive control (Fig. 5 B).

The interaction between CAV1 and TRAF2 was of particular interest. TRAF2 is a stress response protein that colocalizes with and is functionally linked to CAV1, as overexpression of CAV1 promoted TRAF2-mediated downstream signaling in the NF-κB pathway (Feng et al., 2001). Because TRAF2 demonstrated a $CAV1^{Y14\text{-}p}$–dependent interaction with CAV1, a close proximity to CAV1 in cells and, like CAV1, has been proposed to have a role regulating cellular stress signaling. We chose to further investigate this interaction. We first analyzed the compartment in which CAV1 and TRAF2 coassociate. CAV1, when internalized, is known to associate with RAB5-positive early endosomes (Pelkmans et al., 2004; Pelkmans and Zerial, 2005; Hayer et al., 2010; Boucrot et al., 2011). CAV1-GFP colocalized with mCherry-TRAF2 in BFP-RAB5–labeled structures, identifying early endosomes as the major compartment in which TRAF2 and CAV1 coassociate (Fig. 6 A). Next, we performed quantitative PLA using an anti-GFP antibody and antibody to recognize CAV1. The result showed that there was a significant increase in PLA signal in cells coexpressing CAV1-mCherry and GFP-TRAF2 compared with cells expressing GFP-TRAF2 alone, indicating overexpression of CAV1-mCherry increased accumulation of GFP-TRAF2 into CAV1-positive organelles (Fig. S5 A). We next assessed how CAV1 levels affect the subcellular distribution of TRAF2. In control (scrambled siRNA–treated) HeLa cells, mCherry-TRAF2 showed a punctate distribution in the cytoplasm. In contrast, siRNA-mediated reduction of CAV1 levels (Fig. 6 B) resulted in a significant loss of the punctate signal (Fig. 6 C). Expression of CAV1-GFP in the knockdown cells caused a significant increase in the TRAF2 puncta (Fig. 6 D) and demonstrated significant colocalization of CAV1-GFP and mCherry-TRAF2 (quantified in Fig. 6 E).

To further characterize the proposed association of TRAF2 and CAV1, we performed immuno-EM of HeLa cells transfected with GFP-TRAF2 and endogenous CAV1 (Fig. 7). Cells overexpressing GFP-TRAF2 were processed for frozen sectioning and sections immunolabeled for endogenous CAV1 and for GFP. As shown in Fig. 7, specific labeling for GFP-TRAF2 was associated with intracellular compartments including putative tubular and vesicular endosomal elements where it colocalized with endogenous CAV1 (Fig. 7, E, F, and G). The high labeling for endosomal CAV1 in TRAF2 overexpressing cells suggested a redistribution of CAV1 to endosomal compartments and/or stabilization of internal pools of CAV1 (this is also observable in Fig. 8 G). Collectively, these results suggest the mutual interactions between CAV1 and TRAF2 that facilitate the accumulation of CAV1 and TRAF2 in the early endosomal components.

We next investigated the role of CAV1 phosphorylation in TRAF2 association. Antibodies to endogenous $CAV1^{Y14\text{-}p}$ colocalized with mCherry-TRAF2 (Fig. 8 B), suggesting that phosphorylated CAV1 may associate with the early endosomal pool of TRAF2. Cells were then cotransfected with mCherry-TRAF2 and a nonphosphorylated mutant of CAV1, GFP-$CAV1^{Y14F}$. In contrast to WT-CAV1, no colocalization with mCherry-TRAF2 was observed (Fig. 8 C). Collectively, the results suggest that the presence of CAV1 in the early endosomal pathway could facilitate the accumulation of TRAF2 in a $CAV1^{Y14\text{-}p}$ dependent manner.

We next investigated whether stimulation of phosphorylation on $CAV1^{Y14}$ would modulate TRAF2 association. Exposure to H_2O_2 rapidly induces phosphorylation on $CAV1^{Y14}$ in a time- and concentration-dependent manner (Chen et al., 2005). Treatment of HeLa cells for 30 min with 3 mM H_2O_2 triggered an efficient $CAV1^{Y14}$ phosphorylation, as determined

stoichiometric interaction of mCherry-CAV1 and GFP-Fyn at a 7:3 ratio. **(C)** c-Src and CAV1 interact. Left: Codiffusion of GFP–c-Src and mCherry-CAV1. Right: The Gaussian peaks on 0.5 and 0.75 indicated with a dash curve show the subpopulations of stoichiometric interactions between mCherry-CAV1 and GFP-Fyn at 1:1 and 7:3 ratios, respectively. **(D)** eNOS and CAV1 show no detectable interaction. Left: Single-molecule time trace shows GFP-eNOS diffused as monomeric molecules without detectable codiffusion with mCherry-CAV1 in LTE. Right: The histogram shows the Gaussian peak centered on 1, indicating mCherry-CAV1 oligomers in the absence of GFP-eNOS molecules. **(E)** $CAV1^{S80E}$ does not increase interactions of eNOS with the cf-caveolae. The recorded fluorescence signals from both mCherry and GFP were analyzed when as a succession of individual events. The interaction efficiency is calculated from the ratio of GFP fluorescence to the sum of GFP and mCherry fluorescence from each event. This interaction efficiency is counted and plotted as a frequency of events.

Table 1. **Putative CAV1 interactions and CAV1 templates analyzed in this study**

cf-CAV1 templates (mCherry)		
CAV1-FL		
49-101		
S80E		
Y14-p (CAV1 + ABL1 coexpression)		
Putative CAV1 interactors (GFP)		
CSD interactors (CBM)	eNOS	Couet et al., 1997a; García-Cardeña et al., 1997; Sato et al., 2004
	eNOS-CBM domain (N-terminally tagged)	
	eNOS-CBM domain (C-terminally tagged)	
	PTEN	Caselli et al., 2002; Xia et al., 2010
	c-Src	Couet et al., 1997a
	DSG2	Brennan et al., 2012
	RhoA	Gingras et al., 1998
	PPARγ	Burgermeister et al., 2011
Y14-p-dependent interactors	SH2D3C	Boettcher et al., 2010
	GRB10	Boettcher et al., 2010
	VAV2	Boettcher et al., 2010
	GRB2	Boettcher et al., 2010
	TRAF2	Cao et al., 2002
	CSK	Cao et al., 2002
Other putative interactors	Fyn	Wary et al., 1998
	DNM2	Yao et al., 2005
	EHD2	Morén et al., 2012
	Pacsin1	Senju et al., 2011
	Pacsin2	Senju et al., 2011
	LIPE	Aboulaich et al., 2006
eNOS interactor	CALM1	Michel et al., 1997

by immunoblotting with the CAV1$^{Y14\text{-}p}$ antibody (Fig. 8 D). We then used PLA with antibodies directed against endogenous CAV1 and CAV1$^{Y14\text{-}p}$ to detect phosphorylated CAV1 in cells (Fig. 8 E). H_2O_2 treatment caused a significant increase in CAV1 phosphorylation as judged by an increase in the CAV1/CAV1$^{Y14\text{-}p}$ PLA signal (Fig. 8 F). HeLa cells overexpressing mCherry-TRAF2 and treated with H_2O_2 induced a significant colocalization of CAV1$^{Y14\text{-}p}$ with mCherry-TRAF2 on punctate putative early endosomes (Fig. 8 G).

Finally, we sought to confirm the CAV1–TRAF2 interaction with an antibody directed against endogenous TRAF2. To confirm the specificity of the TRAF2 antibody, we performed a Western blot against endogenous TRAF2 and/or overexpressed mCherry-TRAF2. A single band was detected at the estimated molecular weight of endogenous TRAF2 in untransfected cells (Fig. 9 A), and an additional band of predicted molecular weight was observable when cells were transfected with mCherry-TRAF2 (Fig. 9 A). PLA was then performed using anti-TRAF2 and anti-CAV1 antibodies in cells overexpressing GFP-TRAF2 (Fig. 9 B); PLA signals were increased in cells overexpressing GFP-TRAF2 compared with those without transfection. Having validated the antibody pair, we then tested the association of endogenous CAV1 and TRAF2 proteins. Untransfected cells showed a low PLA signal between TRAF2 and CAV1 under control conditions, but this increased significantly after H_2O_2 stimulation (Fig. 9 C). This interaction was specific as negligible PLA signals were obtained using antibodies against Flotillin-1 and TRAF2 with no measurable change upon H_2O_2 treatment (Fig. S5 C). These results confirm colocalization of endogenous TRAF2 and CAV1 and their regulated phosphorylation-stimulated association on early endosomes in response to oxidative stress.

Discussion

cf systems provide a unique opportunity to reconstitute and dissect cellular mechanisms and have proven crucial in elucidation of numerous biological processes (Lingappa et al., 1978; Rothman, 1988). Here we present the first cf system for formation

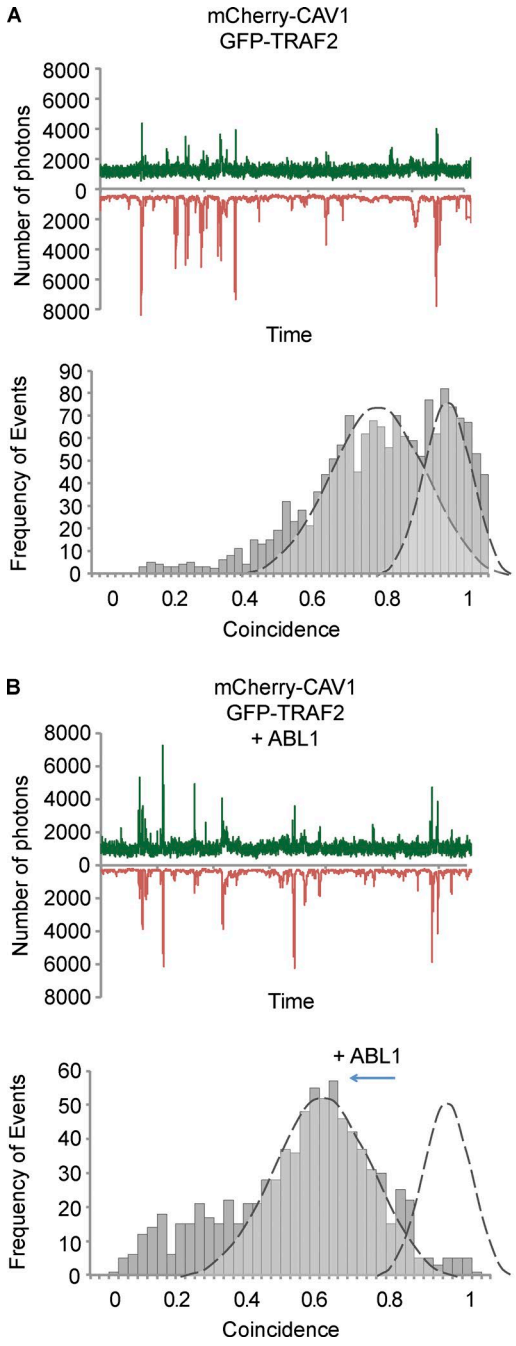

C

Interactors	CAV1FL	CAV1FL + ABL1
CALM1		
CSK		
c-Src	20-30 per caveolae	40-50 per caveolae
DSG2		
DNM2	10-15 per caveolae	10-15 per caveolae
DNM2 K44A		
eNOS		
eNOS CBM(N)		
eNOS CBM(C)		
FYN	15-25 per caveolae	20-30 per caveolae
Pacsin1		
Pacsin2		
PPARγ		
PTEN		
RhoA		
SH2B3		
TRAF2	30-50 per caveolae	100-150 per caveolae
VAV2		
EHD2		
GRB10		
LIPE		

Strongest interaction
Weak Interaction
Sub-stoichiometric
No interaction

Figure 4. **CAV1^{Y14-P} increases interactions of the cf-caveolae with interacting partners. (A)** Individual single-molecule time trace for TRAF2 and CAV1^{FL}. Top: Codiffusion of GFP-TRAF2 and mCherry-CAV1^{FL} shown in coincidence peaks. Bottom: The Gaussian peak on 0.75 indicated with a dashed curve demonstrates the stoichiometric interaction of mCherry-CAV1^{FL} and GFP-TRAF2. **(B)** Single-molecule analysis shows the stoichiometric changes in the interaction between CAV1 and TRAF2 with ABL1 coexpression. Top: When the ABL1 is coexpressed, greater coincidence between GFP-TRAF2 and mCherry-Cav1 is observed. Bottom: The Gaussian peak shifted to 0.6 in the presence of ABL1 shows the stoichiometric interactions between mCherry-CAV1 and GFP-TRAF2 close to a 1:1 ratio. **(C)** CAV1 interaction heat map analyzed by single-molecule spectroscopy. Heat map shows that c-Src, DNM2, Fyn, and TRAF2 interact with CAV1 complexes. Coexpression of untagged ABL1 increased the binding affinity of interacting partners.

of caveolae, one of the most abundant surface organelles of mammalian cells. This system, based on LTE, enables rapid expression, membrane insertion, and curvature generation by CAV1 expressed directly from plasmid DNA. Using high-resolution electron tomography, we have shown that the expression of CAV1 is sufficient to give rise to caveola-like microdomains from endogenous membranes present in the extract. Our findings here demonstrate that cf caveolae-like vesicles closely model native caveolae from mammalian cells. First, striking morphological similarities exist between cf caveolae-like vesicles and native caveolae; EM revealed caveolin-enriched with consistent curvature connected to noncaveolar membrane. Second, membrane association of cf CAV1 resembles CAV1 in native caveolae; the core domains are embedded in the membrane and inaccessible

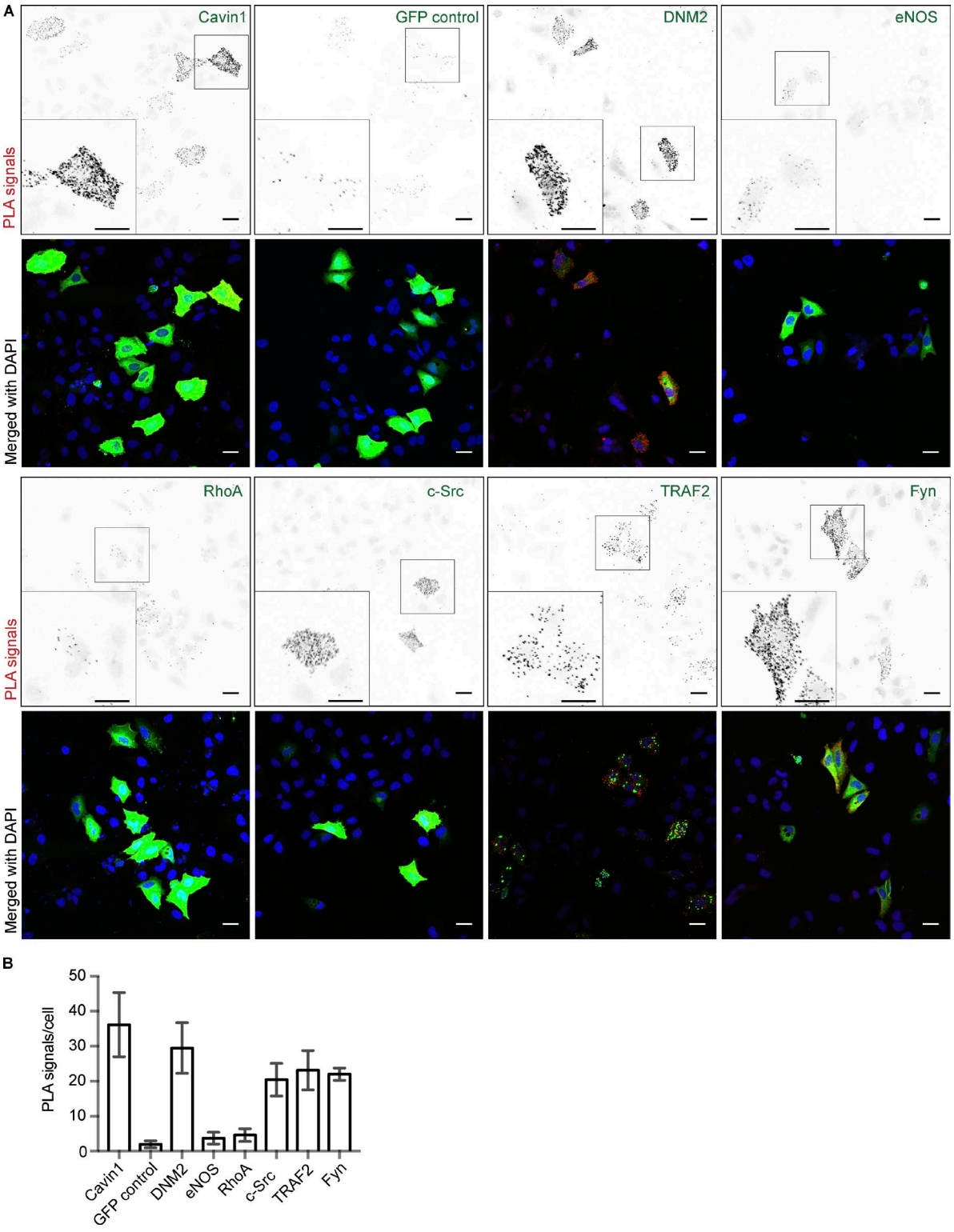

Figure 5. **In vivo validation of CAV1 interactions with GFP-labeled signaling proteins using PLA. (A)** Representative images of PLA between endogenous CAV1 and overexpressed of GFP-tagged Cavin1, GFP alone, DNM2, eNOS, RhoA, Src, TRAF2, and Fyn, respectively. PLA performed using polyclonal anti-CAV1 (rabbit 1:100) and anti-GFP (mouse 1:2,000) primary antibodies. As a positive control, cells transfected with Cavin1 show sharply increased PLA signal (red) with GFP-Cavin1 fluorescence (green). **(B)** Quantification of PLA pairs. Cells transfected with eNOS and PPAR-γ have minimal detectable PLA signal directly comparable to the negative controls indicating no colocalization occurs between CAV1 and these proteins in the cell. Cells transfected with c-Src and TRAF2 have significantly increased PLA signal compared with controls. 30 cells per condition were quantified based on three z-plane images assembled a maximum intensity projection. Data were collected from three independent experiments and expressed as the mean ± SEM. PLA signals were detected as red spots and counted as true signals above a background threshold (~64). Bars, 10 µm.

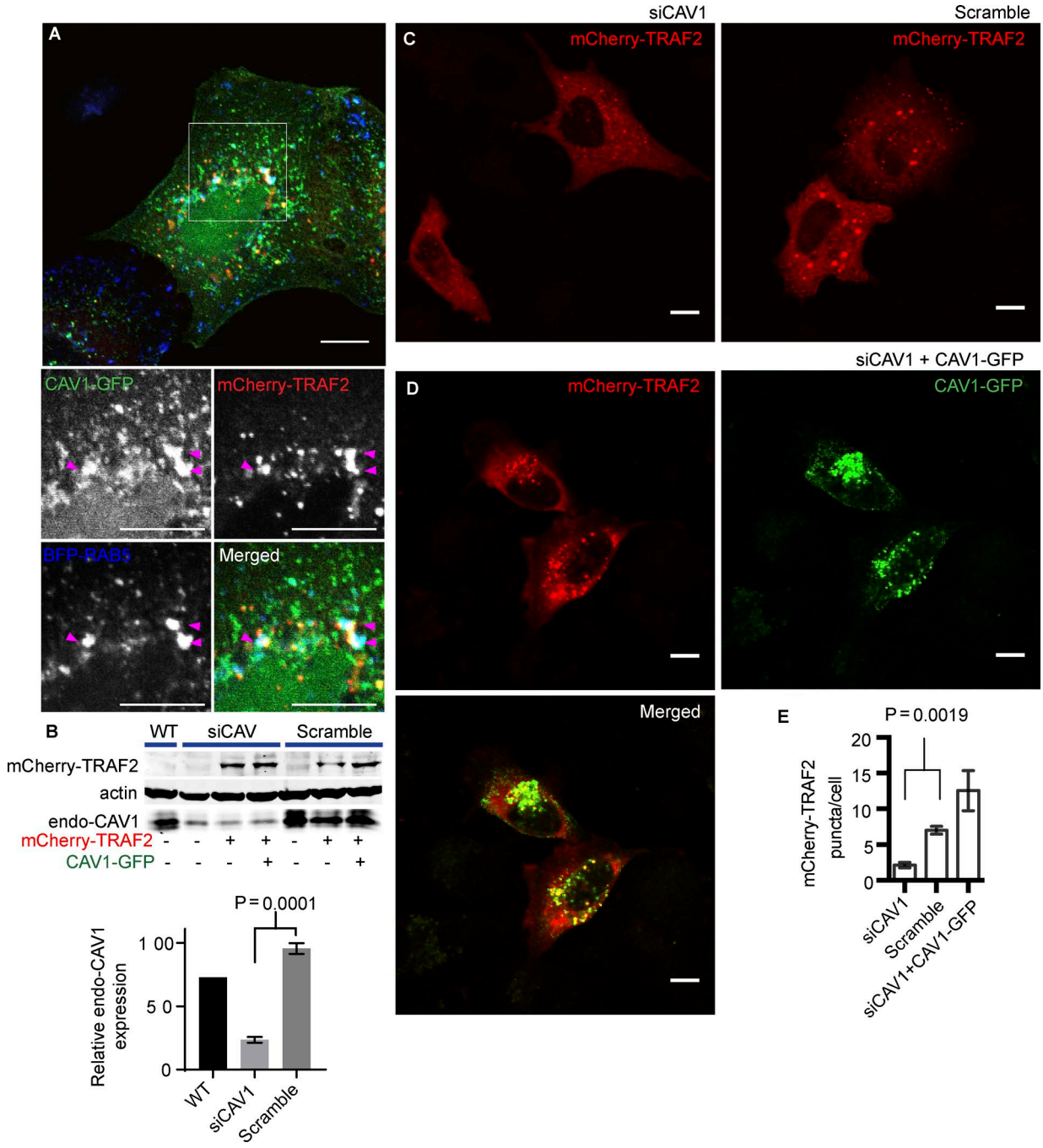

Figure 6. **CAV1-GFP and mCherry-TRAF2 were colocalized to RAB5-positive endosomes. (A)** In HeLa cells overexpressing CAV1-GFP, mCherry-TRAF2, and BFP-RAB5 show that GFP and mCherry fluorescence overlapped in many BFP-RAB5-endosomes. Insets show magnifications of boxed areas. Arrowheads point to endosomal organelles, indicating the presence of colocalization between CAV1-GFP with mCherry-TRAF2 and BFP-RAB5. Bars, 10 µm. **(B)** Immunoblot against CAV1, mCherry, and actin showed that CAV1 knockdown led to significant down-regulation of CAV1 when compared with control cells treated with scramble siRNA (top). Relative endogenous CAV1 expression levels were measured (bottom). Error bars indicate SEM. **(C)** CAV1 knockdown in HeLa-mCherry-TRAF2 cells caused a loss of mCherry-TRAF2 puncta. Cells were treated with siRNA targeting CAV1 and incubated overnight; subsequently, cells were transfected with mCherry-TRAF2. Bars, 10 µm. **(D)** Overexpression of CAV1-GFP in CAV1 knockdown mCherry-TRAF2 HeLa cells led to a redistribution of cytoplasmic mCherry-TRAF2 into a punctate pattern. **(E)** A quantitative analysis of mCherry-TRAF2 puncta in cells with down-regulated CAV1. 30 cells per condition were quantified based on a single confocal slide. mCherry-TRAF2 puncta were detected as saturated spots and counted as true signals above a size threshold (0.5 µm^2). Analysis of the number of mCherry-TRAF2 puncta is shown as the mean ± SEM from three independent experiments.

to protease digestion and, intriguingly, unlike heterologous caveolae generated in *E. coli,* are present in a detergent-resistant lipid environment as in mammalian cells. Finally, using EM analyses of caveolins from different species, we have shown an excellent correlation between caveola formation using our in vitro system and caveola formation in cells. The generation of in vitro synthesized caveolae upon caveolin expression allowed us to investigate the process of caveolar formation and to analyze

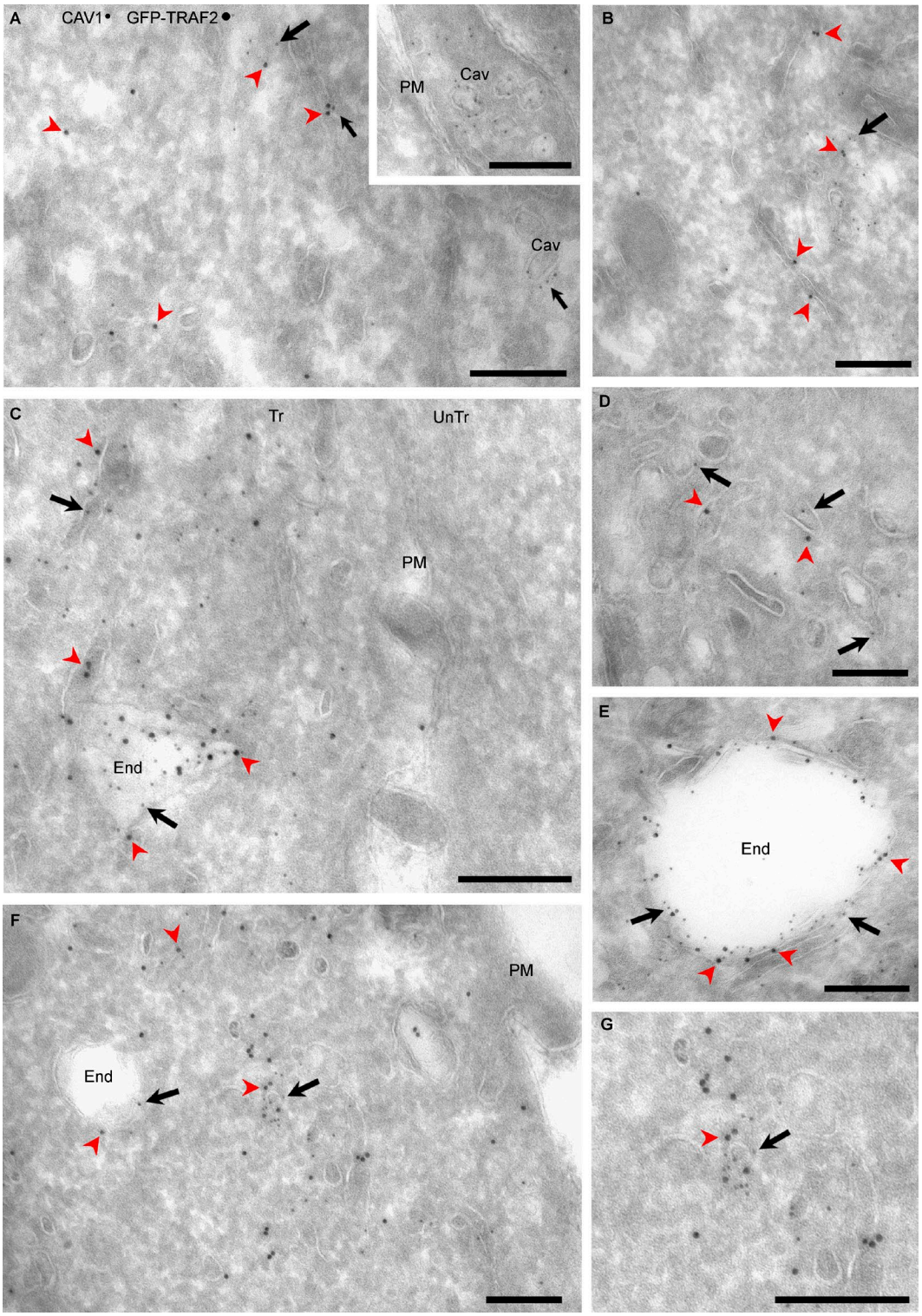

Figure 7. **Immuno-EM localization of expressed TRAF2 (A, B, and D) Low-expressing cells show TRAF2 associated with tubular membranous structures, occasionally in close proximity to CAV1; labeling was rarely observed on CAV1-positive structures, putative caveolae (Cav) close to the plasma membrane (PM; see inset). (C and E–G)** In higher-expressing cells TRAF2 labeling is associated with internal CAV1-positive structures including tubules and structures with endosomal morphology (End). Note the high labeling for endogenous CAV1 in the transfected cells. Panel C shows a transfected cell (Tr) and part of a neighboring untransfected cell (UnTr) demonstrating the specificity of the labeling. G shows a higher magnification of the central area in F and the association of TRAF2 with CAV1-positive structures. Bars, 200 nm. HeLa cells were transfected with GFP-TRAF2 and then processed for frozen sectioning. Sections were labeled with antibodies to endogenous CAV1 (5 nm protein A–gold; black arrows) and GFP (10 nm protein A–gold; red arrowheads).

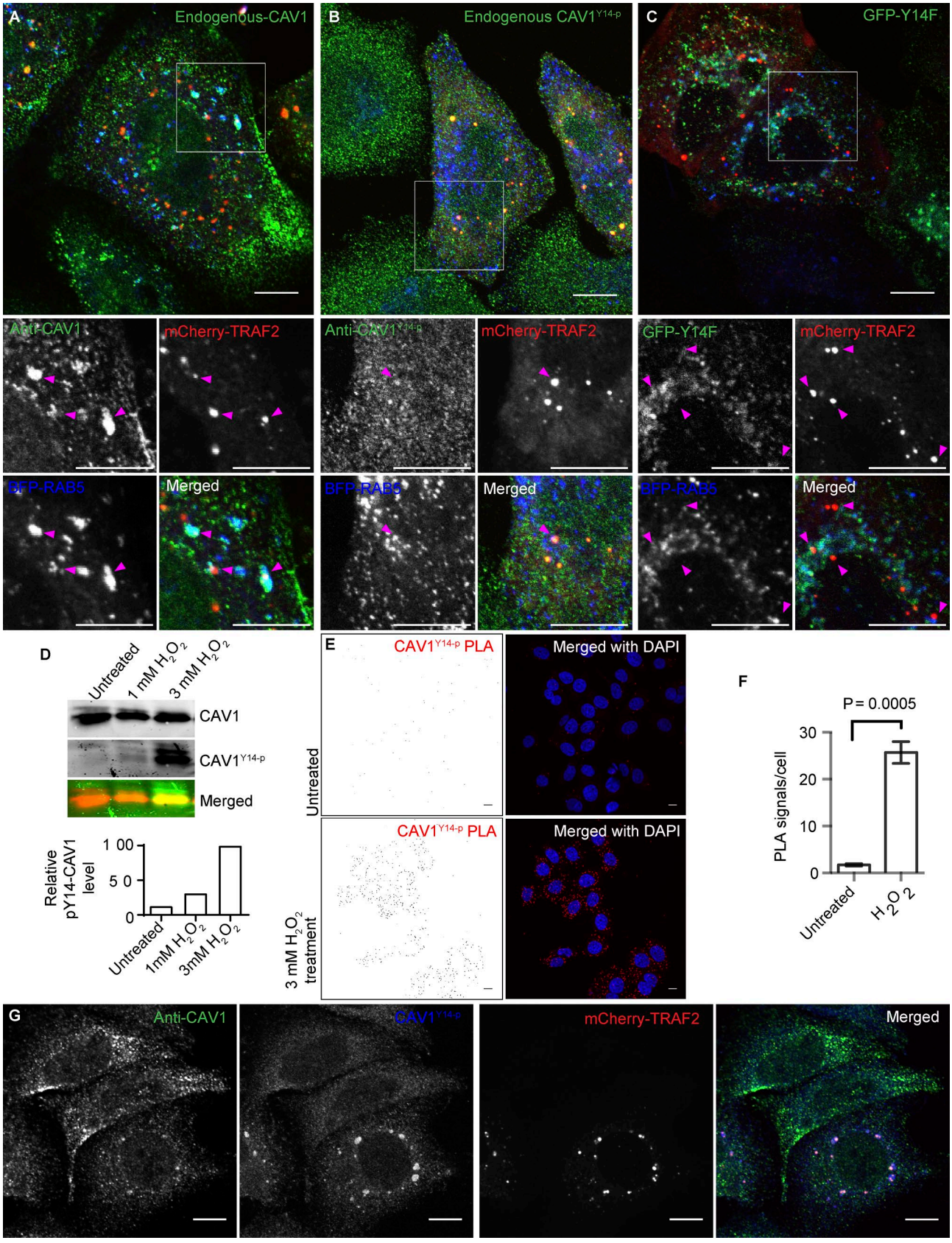

Figure 8. **CAV1 and TRAF2 are colocalized in the endosomal pathway in a phosphorylation-dependent manner. (A)** Endogenous CAV1 and mCherry-TRAF2 were colocalized to RAB5-positive endosomes. In HeLa cells overexpressing mCherry-TRAF2 and BFP-RAB5, the visualization of endogenous CAV1 shows the colocalization of endogenous CAV1 and mCherry-TRAF2 in many BFP-RAB5 endosomes. Insets show magnifications of boxed areas. Arrowheads point to endosomal organelles, indicating the presence of colocalization between endogenous CAV1 with mCherry-TRAF2 and BFP-RAB5. **(B)** CAV1^{Y14-p} is colocalized with

the interactions of membrane-inserted caveolin with target proteins in a high-throughput manner. Although this is a minimal system without the associated cavin coat proteins, EPS15 homology domain–containing (EHD) proteins, and pacsins, it allows us to specifically test the role of direct caveolin protein interactions. An important caveat of our studies is that the interaction of the cavin coat protein, Cavin1, with caveolin inserted into the endogenous membranes within the LTE, is minimal. This is consistent with a model in which cavin association with caveolae involves multiple low-affinity interactions, including with the lipid environment generated by CAV1 (Parton and del Pozo, 2013; Kovtun et al., 2015). Cavins bind both phosphatidylserine and phosphatidylinositol 4,5-bisphosphate (PI(4,5)P2; Mineo et al., 1998; Gustincich et al., 1999; Hill et al., 2008; Kovtun et al., 2015). Phosphatidylserine and cholesterol play a crucial role in caveola formation and stability (Rothberg et al., 1992; Hailstones et al., 1998; Breen et al., 2012; Hirama et al., 2017). The full reconstruction of caveola with coat will therefore require the appropriate lipid composition. The lack of the caveolar lipid environment should therefore be taken into account in studies of interactions with caveolae generated in the in vitro system, especially in the case of negative data. This emphasizes the importance of validating interactions in parallel cellular studies, such as PLA, as used here. In the long term, the cf expression system represents a powerful system in which the lipid composition could be manipulated through the introduction of lipids into the LTE to generate a simple model for formation of a complete caveola.

Mutational and evolutionary analysis of caveola formation

We characterized caveola formation induced by $CAV1^{FL}$ and by a series of cf-expressed CAV1 truncation mutants by a variety of techniques, including single-molecule spectroscopy, sucrose gradient flotation, electron tomography, and biochemical approaches. Expressed $CAV1^{FL}$ generated domains with 100–200 fluorescent particles in a single puncta consistent with the estimated 150–160 CAV1 molecules in a single caveola (Pelkmans and Zerial, 2005; Walser et al., 2012; Sierecki et al., 2014). In agreement with studies on *h*-caveolae generated in *E. coli* (Ariotti et al., 2015), a large portion of CAV1 was protected from cytoplasmic protease digestion consistent with the model that the CSD is tightly juxtaposed to, and the hairpin intramembrane domain is inserted within the membrane. Mutants lacking the N terminus or both N and C termini generated membrane domains with similar numbers of caveolin molecules to the WT protein consistent with the role of the central portion of CAV1, amino acids 81–147, in caveola formation and higher-order oligomerization. The complete loss of membrane association and higher order oligomer formation in a CAV1 mutant missing the putative intramembrane domain indicates the importance of the intramembrane domain for caveola formation. The substitution of Serine80, adjacent to the CSD, to a charged glutamic acid residue (S80E) resulted in the exposure of epitopes within the CSD to protease digestion. This is consistent with the tight membrane association of this domain within caveolae which is perturbed by the addition of a charged residue.

As a test of the cf system to analyze caveola formation, we extended our analysis to a set of evolutionarily distant caveolin species. Caveolins are expressed in vertebrates and some invertebrate species, but it appears that not all caveolins may generate caveolae (Kirkham et al., 2008). For example, caveolin from *C. elegans* was unable to generate caveolae when expressed in mammalian cells yet caveolin from the honey bee, *A. mellifera*, was able to generate morphologically typical caveolae and recruit endogenous cavin proteins (Kirkham et al., 2008). This is consistent with the view that caveolins possess roles outside of caveola formation (Scheel et al., 1999; Kirkham et al., 2008; Schou et al., 2017). Here, we showed that the ability of different caveolins to generate caveolae when expressed in mammalian $CAV1^{-/-}$ cells could be recapitulated in the cf system. The simplicity of cf expression system, involving incubation of the plasmid DNA in the extract and followed by single-molecule analyses or EM, means that caveolin orthologues can be rapidly tested for their ability to generate caveolae as a first step in assessing their role in vivo. Consistent with the previous results in mammalian systems (Kirkham et al., 2008), we showed that caveolin from *A. mellifera* can generate morphological caveolae, whereas *C. elegans* caveolin is integrated into the membrane but lacked the ability to sculpt membranes (Fig. S1 B). This system provides a first step in classifying caveolins from distant branches of evolution as caveogenic or noncaveogenic and represents a powerful, high-throughput system to link caveolin amino acid sequence to CAV1 membrane-sculpting properties.

Analysis of the caveolin interactome using cf caveolae

As a tool for a protein interaction analysis, our cf system brought a technical advance over current methods especially when combined with single-molecule fluorescence analysis. The combination of these techniques allows for systematic quantitative

mCherry-TRAF2. In HeLa cells overexpressing mCherry-TRAF2 and BFP-RAB5, the visualization of $CAV1^{Y14\text{-}P}$ shows colocalization of $CAV1^{Y14\text{-}P}$ and mCherry-TRAF2. Inserts show enlargements of boxed areas. Arrowheads point to the presence of colocalization between endogenous $CAV1^{Y14\text{-}P}$ with mCherry-TRAF2 and BFP-RAB5. **(C)** Phosphorylation on $CAV1^{Y14}$ is required for TRAF2 colocalization at the endosome. In HeLa cells overexpressing phosphodeficient $CAV1^{Y14}$ mutant, $CAV1^{Y14F}$ resulted in the significant loss of the mCherry-TRAF2 colocalization. Inserts show enlargements of boxed areas. Arrowheads point to the presence of mCherry-TRAF2. Bars, 10 µm. **(D)** Temporal $CAV1^{Y14}$ phosphorylation in response to H_2O_2 exposure in HeLa cells. Immunoblot identification of $CAV1^{Y14\text{-}P}$ showed HeLa cells treated with 3 mm H_2O_2 for 30 min triggered efficient phosphorylation on $CAV1^{Y14}$ (top). Relative percentage of the $CAB1^{Y14\text{-}P}$ levels were measured (bottom). **(E)** PLA detection of H_2O_2-induced $CAV1^{Y14\text{-}P}$ in HeLa cells. $CAV1^{Y14}$ was detected by PLA (red dots) in HeLa cells untreated (top) or treated with 3 mm H_2O_2 for 30 min (bottom). The PLA signal was developed with $CAV1^{Y14\text{-}P}$ (1:50) and polyclonal CAV1 (1:100) primary antibodies. **(F)** An increase of the $CAV1^{Y14\text{-}P}$–PLA signal was observed in cells treated with H_2O_2. Thirty cells per condition were quantified based on three z-plane images assembled in a maximum intensity projection. Data were collected from three independent experiments, and PLA signals were detected as red spots and counted as true signals above a background threshold using minimum dark. **(G)** TRAF2 overexpression leads to the accumulation of $CAV1^{Y14\text{-}P}$ in the endosomal pathway in response to oxidative stress. H_2O_2-induced $CAV1^{Y14\text{-}P}$ accumulated and colocalized with mCherry-TRAF2 in endosomes only in mCherry-TRAF2 expressing cells. Bars, 10 µm.

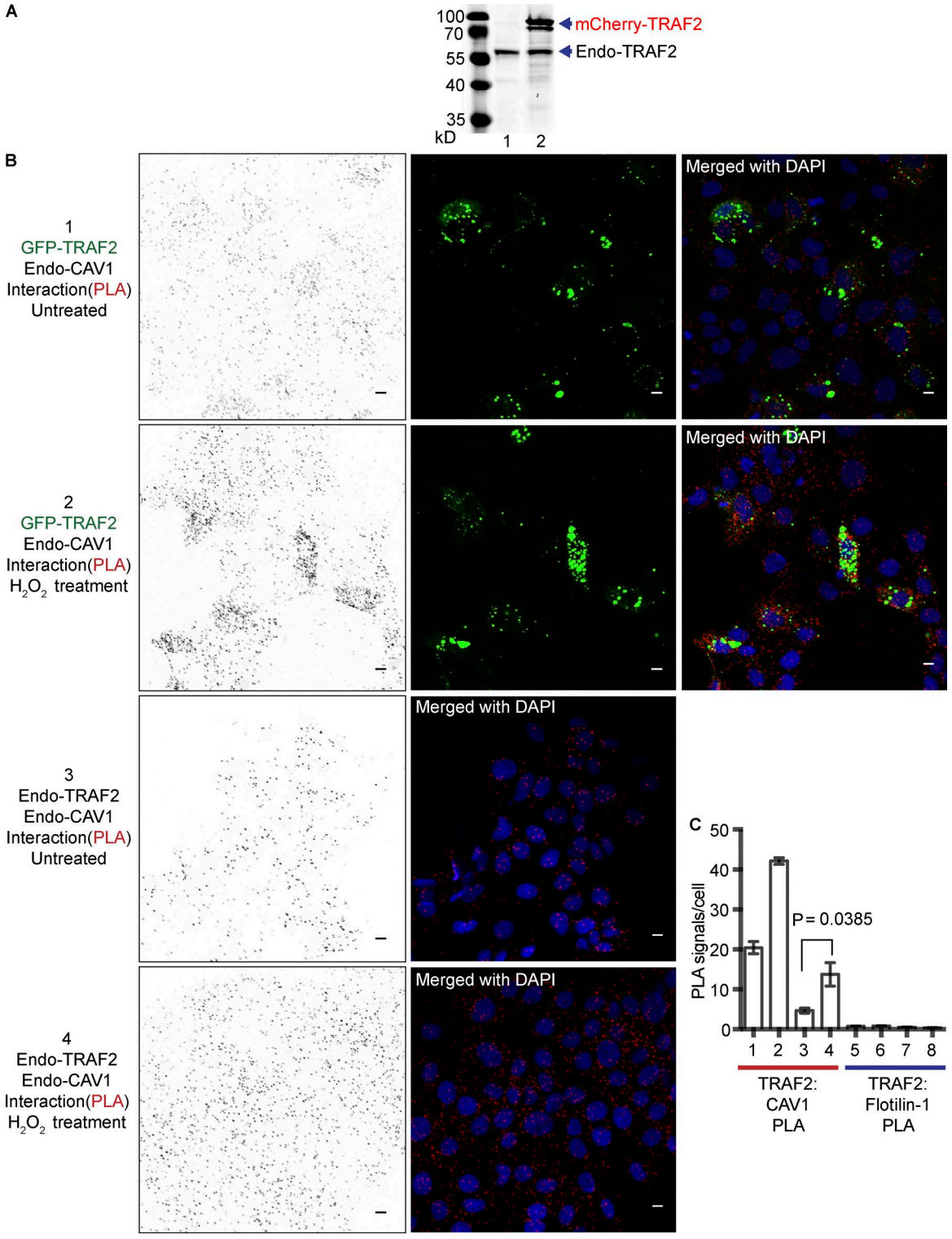

Figure 9. **Quantitative PLA detection of endogenous levels of interactions between CAV1 and TRAF2 in HeLa cells. (A)** Western blot analysis of endogenous and overexpressed TRAF2 expression in HeLa cells. TRAF2 appeared as a single band at ∼56 kD and the transient transfection of mCherry-TRAF2 appeared as a single band at ∼90 kD. Lane 1, untransfected HeLa cell lysate. Lane 2, mCherry-TRAF2-transfected HeLa cell lysate. **(B)** PLA quantification of endogenous CAV1 with either overexpressed TRAF2 or endogenous TRAF2 was performed on untreated or 3 mM H_2O_2-treated cells with antibodies against polyclonal CAV1 (mouse, 1:100) and TRAF2 (rabbit, 1:50). Each PLA spot represents the detection of a protein–protein interaction complex. **(C)** Comparison of PLA quantification between TRAF2:CAV1 (1–4) and TRAF2:Flotillin-1 (5–8). 30 cells per condition were quantified based on three z-plane images assembled in a maximum intensity projection. Data were collected from three independent experiments and expressed as the mean ± SEM. PLA signals were detected as red spots and counted as true signals above a background threshold. Bars, 10 µm.

analysis of protein–protein interactions in a multiwell format and for the determination of stoichiometries of heteroprotein complexes. The use of single-molecule coincidence analysis allowed us to distinguish interactions with higher-order structures of CAV1 from interactions with monomeric soluble CAV1. This allowed the analysis of interactions between membrane-associated oligomeric CAV1 characteristic of caveolae and potential target interacting proteins.

Until recently, the physical interaction between the CSD of caveolin and the caveolin binding motifs (CBMs) of numerous signaling proteins was a well-established dogma in the field (Couet et al., 1997a; Okamoto et al., 1998). This, however, was despite a lack of understanding of how an apparently constitutive protein–protein interaction could be reversibly regulated in cells. More recent works have challenged the validity of this model (Byrne et al., 2012; Collins et al., 2012). We assayed direct protein–protein interactions in a model system that can discriminate between caveolin embedded within a membrane from a soluble form of CAV1 to identify interactions with the oligomeric caveolin characteristic of caveolin within caveolae. Using this system, we observed no significant interaction between CAV1 and several proteins containing CBMs, including PPAR-γ, PTEN, RhoA, and DSG2 (Gingras et al., 1998; Caselli et al., 2002; Xia et al., 2010; Burgermeister et al., 2011; Brennan et al., 2012). This was further confirmed using PLA in cells. Together with previous studies involving bioinformatics and structural analyses, which showed that CBMs (1) do not adopt a common structure for scaffolding domain association, (2) are not available for direct protein–protein interactions, and (3) are not specifically enriched in the caveolin interactome (Byrne et al., 2012; Collins et al., 2012). These observations are consistent with our findings that suggest that CBM- and CSD-dependent interactions are unlikely to occur.

This result is particularly surprising for the proposed interaction of CAV1 with eNOS. CAV1 has been functionally linked to eNOS in numerous studies, both in cell culture systems and in vivo, and peptides derived from the CSD show potent and specific effects on eNOS in vitro and in vivo (Couet et al., 1997a; García-Cardeña et al., 1997; Ju et al., 1997; Gratton et al., 2003; Sato et al., 2004; Bernatchez et al., 2005). However, together with previous analyses (Byrne et al., 2012; Collins et al., 2012), the mechanisms involved in these effects must clearly be reexamined. We did not observe any interaction between eNOS and CAV1, despite showing a specific and calcium-dependent interaction of eNOS and CALM1 using the same cf expression system. Single-molecule coincidence indicated eNOS has no detectable affinity for membrane associated $CAV1^{WT}$, nor with the CSD accessible $CAV1^{S80E}$. Consistent with our single-molecule data, the PLA assay between CAV1 and eNOS showed no significant signal above that obtained with the soluble GFP control. To assess the CBM peptide based analysis, we made and characterized constructs exposing the CBM of eNOS on either the N terminus or C terminus of soluble GFP, showing no measurable affinity for $CAV1^{WT}$ and $CAV1^{S80E}$. This result suggests that the CSD does not interact with the CBM of eNOS. Collectively, our cf assays clearly show that direct protein interactions between CSD and CBM are unlikely to occur and, therefore, that the central tenet of the model needs to be revaluated. This, however, does not rule out an important role for CAV1 in eNOS regulation, but rather indicates this regulation may occur through more complex mechanisms. A recent study revealed the possibility that eNOS activation is linked to alteration of membrane order or cholesterol-enriched domains, not individual caveolae (Tran et al., 2016). In agreement with this, alterations in caveolar components have been shown to influence lipid-based signaling pathways (Ariotti et al., 2014) and the CSD has been shown to affect clathrin-independent endocytosis and membrane lipid mobility (Hoffmann et al., 2010; Chaudhary et al., 2014). The CSD contains a potential cholesterol recognition and interaction amino acid consensus motif (Li and Papadopoulos, 1998; Sun et al., 2007), leading to the possibility that administration of CSD-peptide could induce a global change in membrane dynamics. We speculate that eNOS activation is not controlled directly by CAV1 via the proposed CSD–CBM interaction, but by the global membrane order controlled by CAV1.

As an alternative to the direct interaction caveolin signaling hypothesis, $CAV1^{Y14}$ is also proposed to induce signaling protein interactions upon phosphorylation. Multiple papers proposed $CAV1^{Y14\text{-}p}$ as a potential binding motif for SH2 domain–containing proteins (Lee et al., 2000; Boettcher et al., 2010; Park et al., 2015). To test $CAV1^{Y14\text{-}p}$ protein interactions, we developed an in vitro tyrosine-phosphorylation method where the coexpression of ABL1 kinase with CAV1 is sufficient to induce phosphorylation of CAV1 in this system (Fig. S4 D). Our data showed the $CAV1^{Y14\text{-}p}$ promoted interaction with the SH2 domain–containing proteins, c-Src, and Fyn (Fig. 4 C). We believe that $CAV1^{Y14\text{-}p}$ is a potential docking site for SH2 domain–containing proteins which can be regulated by Src family kinases. However, further studies are required to demonstrate the role and the molecular mechanism of SH2 domain–containing protein interactions.

Phosphorylation regulated interaction of caveolin-1 with TRAF2

We identified several interacting partners of oligomerized CAV1 including the Src kinase Fyn, DNM2, and TRAF2. Furthermore, we established systems to phosphorylate CAV1 in vitro to allow analysis of the role of Y14 phosphorylation in regulating these interactions. Coexpression of ABL1 kinase with CAV1 was sufficient to induce phosphorylation of >50% of the total CAV1. These systems were used to examine the potential interaction of CAV1 and TRAF2. Single-molecule coincidence analyses revealed a coincidence peak from both proteins and the coincidence peak significantly increased when the $CAV1^{Y14}$ was phosphorylated by ABL1 coexpression. A role for CAV1 in TNF-signaling was first suggested by the demonstration that TRAF2 and CAV1 could be coimmunoprecipitated (Feng et al., 2001). Overexpression of CAV1 increased the protein levels of overexpressed TRAF2 and enhanced TRAF2-mediated NF-κB signaling (Feng et al., 2001). Subsequent studies showed a $CAV1^{Y14\text{-}p}$–stimulated TRAF2 interaction using a yeast hybrid system (Cao et al., 2002).

Our cellular studies validated our newly developed cf approach but extended the earlier identification of TRAF2 as a CAV1-interacting protein (Feng et al., 2001; Cao et al., 2002). Our studies suggest a role for CAV1 phosphorylation in TRAF2 regulation at the level of the early endosome. CAV1 phosphorylation was stimulated by hydrogen peroxide treatment, leading to the endosomal localization of CAV1, where it triggers TRAF2

accumulation. Reduction of CAV1 levels caused a redistribution of TRAF2 that was rescued by reexpression of CAV1 suggesting that caveolin may act as a scaffold for TRAF2 recruitment to the early endosome. Concomitantly, TRAF2 overexpression induced global changes to endogenous CAV1 distribution and enrichment within the endosomal compartment (Fig. 7 and Fig. 8 G). We believe that this endosomal accumulation of CAV1-TRAF2 leads to the stabilization of these proteins to activate signaling pathways. Consistent with this idea, TRAF2 deficiency in cells has been shown to affect H_2O_2-induced JNK activation (Shen et al., 2004), and phosphorylation on CAV1^{Y14} has been shown to be a key step for JNK activation when cells are treated with paclitaxel, an antimicrotubule-disrupting drug (Shajahan et al., 2012). TRAF2 has been suggested to be a potential activator in the NF-κB signaling pathway with the transient colocalization and interaction of TRAF2 and APPL1 in the early endosomes being involved in de novo signaling (Hupalowska et al., 2012). As rapid phosphorylation of CAV1^{Y14} occurs in response to many different stress stimuli (Li et al., 1996b; Aoki et al., 1999; Volonté et al., 2001; Zhang et al., 2007; Joshi et al., 2012) the phosphorylation-dependent interaction of TRAF2 and CAV1 may represent a general response to cellular stress.

Materials and methods

The library of *Leishmania* expression vectors

The open reading frames (ORF) were sourced from the ARVEC Facility, UQ Diamantina Institute, and cloned into the *Leishmania* expression vectors. In brief, the ORFs were exchanged with the *ccdB* gene in the pDONOR221 vector by BP recombination (Invitrogen), and then the pDONOR221 encoding ORF was subjected to the gene exchange with destination vectors: pCellFree-N-terminal-GFP and pCellFree-N-terminal-Myc-Cherry by LR recombination (Invitrogen). The list of coding sequences were as follows: ABL1 (VDNA142B6), CALM1 (VDNA042H4), c-Src (VDNA087F5), CSK (BC104847), DNM2 (BC039596), DSG2 (VDNA157G9), EHD2 (VDNA132E8), eNOS (VDNA127E1), Fyn (VDNA065G7), GRB2 (VDNA019H2), GRB10 (VDNA207E6), LIPE (VDNA121H6), Pacsin1 (VDNA063D2), Pacsin2 (VDNA076H3), PPAR-γ (VDNA065D3), PTEN (VDNA188B2), RhoA (VDNA075D9), SH2D3C (VDNA071G10), TRAF2 (VDNA067A4), and VAV2 (VDNA183C11).

Generation of plasmid pEGFP-N1-Cavin1 for mammalian Cavin1-GFP expression was previously described (Hill et al., 2008). To generate a mammalian TRAF2 expression vector yielding N-terminal fusion of GFP or mCherry, the coding sequence for TRAF2 (VDNA067A4; UQ Diamantine) was cloned into pEGFP-C1 or pmCherry-C1, respectively (BD; Clontech) as EcoRI–BamHI fragment. PCR amplification of TRAF2 flanked by EcoRI–BamHI sites was performed with appropriate primers as follows: TRAF2 forward, 5′-GCTCAAGCTTCGAATTCTATGGCTGCAGCTAGCGTG ACC-3′; TRAF2 reverse, 5′-AGATCCGGTGGATCCTTAGAGCCCTGT CAGGTCCACAATGGC-3′.

To generate BFP-RAB5 in a mammalian expression vector, the coding sequence for BFP (Subach et al., 2008) was cloned into the pEGFP-C1-RAB5 vector by replacing the coding sequence for GFP with BFP as an AgeI–EcoRI fragment. PCR amplification of BFP flanked by AgeI–EcoRI sites was performed with appropriate primers as follows: BFP forward, 5′-CCCGGGATCCACCGGTCG CCACCATGAGCGAGCTGATTAAGGAGAACA-3′; BFP reverse, 5′-CTAGCCATCGGAATTCGAAGCTTGTGCCCCAGTTTGCTA-3′.

Preparation of LTE

Cultures (*Lt*) were grown in TB medium (tryptone 12 g/liter, yeast extract 24 g/liter, glycerol 8 ml/l, glucose 1 g/liter, KH_2PO_4 2.31 g/liter, and K_2HPO_4 2.54 g/liter) at 26°C to a final OD_{600} of 1.9 and harvested cells were pelleted at 2,500 g for 5 min. Cells were washed once in resuspending buffer (45 mM Hepes-KOH, pH 7.6, 250 mM sucrose, 100 mM KOAc, and 3 mM $Mg(OAc)_2$) and resuspended with the cell concentration at 10^{10} cells/ml. Next cells were lysed by cell disruption using a nitrogen cavitation device (70 bar N_2, 45-min equilibration at 4°C). The cell lysate was then centrifuged at 10,000 *g* for 15 min and the top 2/3 supernatant was carefully recovered, followed by a sequential centrifugation at 30,000 *g* for 15 min, followed by a recovery of 2/3 supernatant. The recovered supernatant was then subjected to gel filtration over a desalting gel (PD-10; GE Healthcare) with elution buffer (45 mM Hepes-KOH, pH 7.6, 100 mM KOAc, and 3 mM $Mg(OAc)_2$) and supplemented with antisplice leader oligonucleotide (5′-CAATAAAGTACAGAAACTGATACTTATATAGCG TT-3′) at 0.05 Mm (Mureev et al., 2009).

Caveolin expression in a cf protein system

Protein of interest (POI) was translated in LTE as previously described in detail (Kovtun et al., 2011). The purified DNA template was adjusted with mQ water to make up a final concentration of 20 nM in the translation mix containing 50% of LTE supplied with 20% of feeding solution containing cofactors and enzymes (0.5 mg/ml T7 RNA polymerase, 200 U/ml creatine phosphokinase, and 5.25× protease inhibitor [cOmplete EDTA-free; 1187358001; Roche Life Science], 2.5 mM rNTP mix, 0.68 mM of each amino acid, 200 mM creatine phosphate, 6 mM ATP, 0.68 mM GTP, 22.5 mM $Mg(OAc)_2$, 1.25 mM spermidine, 10 mM DTT, 5% [vol/vol] PEG 3000, and 100 mM Hepes-KOH, pH 7.6; Kovtun et al., 2011). The reactions were incubated at 27°C for 2 h. Fluorescence readout of the translation mix was performed to monitor the level of translation. Translation mixtures (20 µl) were loaded into 384-well white plates and GFP fluorescence (520-nm emission) was recorded every 4 min using 485-nm excitation lasers in a plate reader (Synergy 4; BioTek).

For translational fluorescent labeling, BODIPY-FL-Lys-tRNA (UUU; Fluoro Tect; Promega) was added to the translation mix at 1:200 ratio. After 2 h of incubation at 27°C, the 4-µl aliquot of reactions were subjected to SDS PAGE and visualized on a Chemi-Doc XRS+ system (Biorad) using 488-nm excitation source and 520-nm detector.

AlphaScreen assay

The AlphaScreen Assay was performed using the cMyc detection kit (Perkin Elmer) as previously described (Sierecki et al., 2014). Samples were subjected to a fourfold serial dilution in buffer A (25 mM Hepes and 50 mM NaCl) and 2 µl of diluted samples were aliquoted into Proxiplate-384 Plus plate (Perkin Elmer) with 12.5 µl (0.4 µg) of anti-cMyc–coated acceptor beads in buffer B (25 mM Hepes, 50 mM NaCl, 0.001% vol/vol casein,

and 0.001% vol/vol Nonidet P-40), and then, 2 µl biotin-labeled GFP nanobody in buffer A was added to make up a final concentration of 2.5 nM, followed by incubation for 45 min at RT. This was followed by the addition of 2 µl (0.4 µg) streptavidin-coated donor beads in buffer A and then a second incubation for 45 min at RT in the dark. The AlphaScreen signal was recorded on the PE Envision Multilabel Platereader using the 680-/30-nm excitation source for 0.18 s and 570/100FF-nm detector after 37 ms.

Single-molecule spectroscopy

Single-molecule spectroscopy was performed as previously described (Sierecki et al., 2014). Samples were diluted in buffer A to a final concentration of ∼1 nM and loaded (20 µl) into a customized silicone 192-well plate equipped with a 70- × 80-m glass coverslip (ProSciTech). Sample plates were analyzed with one laser (488 nm) for autocorrelation, or two lasers (488 nm and 561 nm) for cross-correlation using a homemade single-molecule detection setup. The lasers were focused in the sample solution using a 40×/1.2 NA water-immersion objective (Zeiss). The fluorescence emission was filtered with 500- to 550-nm band pass filter (GFP), and with 580 nm long-pass filter (mCherry).

For single-molecule burst brightness analysis, the frequency of events for each range of GFP fluorescence intensity was counted and plotted on a histogram.

For single-molecule coincidence measurements, CAV1 and partner proteins were coexpressed in the LTE and were diluted in buffer A. The single-molecule events were recorded in 1-ms time bins. To quantify and measure the efficiency of interactions, we analyzed the interaction coincidence (C) of an individual subpopulation in the sample. When analyzing the binding of proteins onto cf caveolins, we selected the high-intensity peaks corresponding to the diffusion of "caveolae" by thresholding the signal at 500 photons/ms. For each peak above this threshold, we calculated the stoichiometry of interaction as

$$C = \frac{\text{mCherry fluorescence}}{(\text{GFP fluorescence} + \text{mCherry fluorescence})}.$$

The set of values of interaction efficiency obtained from the experiments are rational numbers between 0 and 1. At the time point, if the GFP fluorescence is high the value will skew toward 0, and conversely, if the mCherry fluorescence is high, the value will skew toward 1. If both GFP and mCherry fluorescence are high the value will be close to 0.5. Therefore, the Gaussian peaks from 0 and 1 represent the GFP only and mCherry only oligomeric complexes, respectively, whereas the Gaussian peak between 0.25 and 0.75 represent the codiffusion of GFP- and mCherry-tagged proteins in complexes. The individual value was plotted in a histogram allowing determination of the stoichiometry of the protein interactions.

Gradient floatation fraction assay

GFP-tagged caveolin WT and truncation mutants were expressed (75 µl each) in the presence of a lipid dye, DiIC16 (D384; Invitrogen; at 1:1,000 dilution), and mixed with an equal volume of 80% (wt/vol) Histodenz (Sigma-Aldrich) solution in PBS. The mixed samples were loaded at the bottom of 11 × 22 mm Beckman centrifuge tubes (Beckman Instrument). The tube was sequentially overlaid with a linear Histodenz gradient (7.5%–37.5% wt/vol) in PBS. Gradients were spun at 150,000 *g* for 16 h in a TLS-55 rotor (Beckman Instrument) at 4°C. After that, samples were collected from the top in 50-µl increments and loaded into 384-well white plates. Fluorescence levels of GFP and DiIC16 for each fraction were read on a plate reader (Synergy 4; BioTek; excitation 485 nm and emission 520 nm for GFP and 549 nm/575 nm for DiIC16, respectively).

SDS PAGE and Western blot

Solubilized samples with sample buffer (45 mM Tris-HCl, 10% glycerol, 1% SDS, 0.01% [wt/vol] bromophenol blue, and 2% β-mercaptoethanol) were boiled at 95°C for 5 min and subjected to SDS PAGE (10% polyacrylamide gel with 4% stacking gel; running buffer –25 mM Tris, 250 mM glycine, and 0.1% SDS) and then transferred to an Immobilon-P membrane (Millipore), using 1× transfer buffer (48 mM Tris, 39 mM glycine, and 20% methanol). For immunodetection, membranes were blocked with blocking buffer (5% BSA in TBST buffer [50 mM Tris, 150 mM NaCl, and 0.1 % Tween 20, pH 7.6]) for at least 4 h at 4°C and incubated with various primary antibodies; polyclonal CAV1 antibody (1:5,000; 610406; BD Transduction Laboratories), CAV1 (N20) antibody (1:2,000; SC-894; Santa Cruz Biotechnology), TRAF2 antibody (1:100; EPR6048; Abcam), VIP-N antibody (1:2,000), Concav antibody (1:2,000), Myc-rabbit antibody (1:1000; 71D10; Cell Signaling technology), GFP antibody (1:5,000; 11814460001; Roche Life Science), and CAV1$^{Y14\text{-}P}$ antibody (1:100; 611338; BD Transduction Laboratories) in incubation buffer (2.5% BSA in TBST) for overnight at 4°C, followed by the secondary horseradish peroxidase–conjugated antibody incubation (1:10,000) for 1 h at RT. The bands were visualized by using Super Signal West Pico dura chemiluminescent substrate (Pierce) according to manufacturer's instruction on a ChemiDoc XRS+ system (Biorad).

Protease protection assay

Samples were diluted in PBS (0.5 mg/ml) and incubated with ProK enzyme (at 1:1,000 dilution; New England Biolabs) at 37°C for 30 min. For the detergent pretreatment, samples in PBS were incubated with Triton X-100 (0.5% final dilution) or SDS (0.1% final dilution) at 37°C for 30 min with mild agitation, followed by ProK incubation with mild agitation. After the digestion, the samples were subjected to SDS PAGE and Western blot for further analysis.

EM

For immunogold labeling of LTE, samples were incubated on glow-discharge carbon coated grids by 20 min. After blocking with 1% casein in PBS 3 times for 5 min, the samples were targeted by GFP nanobody-MBP (60 µg/ml) in the blocking buffer followed by anti-MBP antibody rabbit IgG (at 1:100 dilution; New England Biolabs). The bound antibodies were visualized with 10 nm colloidal gold-conjugated protein A (at 1:50 dilution; Cell Microscopy Center, Department of Cell Biology, University Medical Center, Utrecht, Netherlands).

For negative staining, samples were adhered to EM grids, fixed with 4% PFA in PBS for 10 min, washed with PBS, and stained with methylcellulose and uranyl acetate (9:1) for 10 min. The samples were observed at 80 kV in a electron microscope (JEOL 1011; Japan) and imaged under the control of the Morada Soft Imaging System (Olympus).

For electron tomography, Cf-caveolin-containing membranes were adhered to EM grids and subjected to immunogold staining and subsequent negative staining. Dual-axis tilt electron tomography was performed (−60° to 60° at 2° incremental sampling) using a TECNAI 12 microscope (Philips) at 120 kV fitted with a 4,000 × 4,000 LC-1100 Direct Electron under the control of SerialEM (Boulder, CO) at twofold binning. The densities of cf-caveolin–containing membranes were reconstructed from tilt series using weighted back-projection in IMOD (Boulder, CO).

For immuno-EM on frozen sections, HeLa cells expressing GFP-TRAF2 were fixed in 4% PFA and 0.2% glutaraldehyde in PBS. Fixed cells were scraped then embedded in 2.3 M sucrose and frozen on pin stubs in liquid nitrogen. 70-nm ultrathin sections were cut on a Leica FCS6 at −120°C. Sections were washed in PBS, quenched, blocked in 0.1% fish skin gelatin and 0.1% BSA in PBS and then subjected to sequential labeling. Sections were incubated with a rabbit primary antibody directed against CAV1 (1:200; 610406; BD Transduction Laboratories) for 30 min, washed, incubated with 5 nm colloidal gold-conjugated protein A (at 1:50 dilution; Cell Microscopy Center, Department of Cell Biology, University Medical Center, Utrecht, Netherlands). Sections were washed again, fixed in 0.1% glutaraldehyde and subjected to a second round of labeling with anti-GFP rabbit (1:200) and 10 nm colloidal gold-conjugated protein A (at 1:50 dilution). The samples were observed at 80 kV in a electron microscope (JEOL 1011; Japan).

Protein kinase assay

To identify the CAV1^{Y14} as an ABL substrate in LTE, GFP-tagged CAV1 was coexpressed with GFP-tagged ABL1 or ABL2 kinase (8:2) in 50 µl of reaction mixture with or without the addition of phosphatase inhibitor after 40 min of initial reaction (PhosSTOP; 4906837001; Roche Life Science). The samples were then incubated with GFP nanobody cross-linked Sepharose beads for 30 min at 4°C with mild agitation, followed by ice-cold PBS (300 µl) washing three times. The sample was eluted by adding 20 µl of boiling SDS sample buffer containing 20 mM 2-Mercaptoethanol, then processed for Western blotting. The phosphorylated CAV1 bands were detected by purified mouse anticaveolin (CAV1$^{Y14\text{-}p}$; 611338; BD Transduction Laboratories).

Quantification of CAV1$^{Y14\text{-}p}$

GFP-tagged CAV1 was coexpressed with GFP-tagged ABL1 (8:2) in 1 ml of reaction mixture with the addition of phosphatase inhibitor after 40 min of initial reaction (PhosSTOP; 4906837001; Roche Life Science). The caveolin-positive vesicles were purified using the gradient density assay as described above and solubilized by adding 10% (vol/vol) of ×10 RIPA buffer (25 mM Tris pH 7.6, 150 mM NaCl, 1% NP-40, 1% sodium deoxycholate, and 0.1% SDS). CAV1$^{Y14\text{-}P}$ was immunoprecipitated using purified mouse anticaveolin (CAV1$^{Y14\text{-}p}$; 611338; BD Transduction Laboratories)–coupled protein A beads and processed for SDS PAGE and Western blot subsequently as a positive control (IP-CAV1$^{Y14\text{-}p}$). To find the optimized condition for CAV1$^{Y14\text{-}p}$, a series of different ratios of ABL1 and CAV1 templates (3:7, 5:5, 7:3, and 9:1, respectively) was tested in the 100-µl reaction mixture (total 20 nM of DNA templates in final volume) in the presence of phosphatase inhibitor (PhosSTOP; 4906837001; Roche Life Science). The samples were then incubated with GFP nanobody cross-linked Sepharose beads for 30 min at 4°C with mild agitation, followed by ice-cold PBS (300 µl) washing three times. The sample was eluted by adding 20 µl of boiling SDS sample buffer containing 20 mM 2-Mercaptoethanol, then processed for SDS PAGE and Western blot subsequently. Afterward the proteins were analyzed by quantitative Licor Western blotting (Odyssey, LI-COR) with antibodies specific to CAV1$^{Y14\text{-}p}$ and total CAV1 (Polyclonal CAV1 antibody; 610406; BD Transduction Laboratories). The relative phosphorylation levels were measured by comparing the phosphorylated and total CAV1 bands after normalization of the IP sample bands (IP-CAV1$^{Y14\text{-}p}$).

Phylogenetic analysis

Phylogenetic analysis was performed with Neighbor Joining method from the alignment of caveolin sequences as indicated using Vector NTI AlignX 9.0 software (Thermo Fisher Scientific).

Cell culture and transfections

HeLa cells (American Type Culture Collection) were grown in DMEM supplemented with 10% FCS. HeLa cells were transfected with Lipofectamine 3000 (Invitrogen) as per the manufacturer's instruction and incubated for at least 24 h before process.

PLA analysis in cultured HeLa cells

HeLa cells (American Type Culture Collection) were grown on coverslips and cultured in DMEM containing 10% FCS. Cells were transfected with Lipofectamine 3000 (Invitrogen) as per the manufacturer's instruction and incubated 24 h before processing. Cells were washed with ice-cold PBS three times and fixed with 4% PFA in PBS for 15 min at RT. After ice-cold PBS washing three times for 3 min, cells were permeabilized with using 0.1% Triton X-100 in PBS for 15 min, washed with ice-cold PBS five times for 3 min, and then incubated with PLA blocking buffer overnight at 4°C. The next day, the cells were washed with PBS three times for 5 min and incubated with the following combinations of antibodies in blocking buffer overnight at 4°C: anti-GFP mouse, at a dilution of 1:2,000 and anti-CAV1 rabbit (N20) 1:100; anti-CAV1PY14-p mouse, 1:50 and anti-CAV1 rabbit (N20), 1:100; anti-CAV1 mouse, 1:100 and anti-TRAF2 rabbit, 1:50; anti-flotillin-1 mouse, 1:100 and anti-TRAF2 rabbit, 1:50. PLA assay was performed after primary antibody incubation using the Orange detection kit according to the manufacturer's instructions (Olink Bioscience) including secondary probe incubation, ligation, and amplification. When the two primary targets were within 40 nm, the secondary proximity probes hybridized and offered a concatemeric DNA template, leading to amplification of PLA signal. Followed by mounting coverslips with Duolink mounting medium with DAPI (Olink Bioscience). Confocal images were collected using ZEN software on an upright confocal microscope

(LSM 710; Carl Zeiss; Plan Apochromatic 20×/0.8 M27 objective) with a color camera (DP-71 12 Mp). 30 cells per condition were quantified based on three z-plane images assembled into a maximum intensity projection using ImageJ software (The National Institutes of Health) and automatic particle counting above a threshold of 0.5 μm^2 in size. PLA signals were detected as red puncta and counted above an intensity threshold value (65~).

Cell culture, transfections, and siRNA-mediated down-regulation of CAV1

HeLa cells (American Type Culture Collection) was grown in DMEM supplemented with 10% FCS. HeLa cells were transfected with Lipofectamine 3000 (Invitrogen, Australia) as per the manufacturer's instruction and incubated at least 24 h before processing. The transient CAV1 knockdown in HeLa cell line was accomplished using stealth siRNA (CAV1HSS141466; Invitrogen) at 50 nM with Lipofectamine 3000 (Invitrogen). After 24 h incubation, cells were subsequently transfected with mCherry-TRAF2 or cotransfected with mCherry-TRAF2 and CAV1-GFP by Lipofectamine 3000 (Invitrogen, Australia) as per the manufacturer's instruction and incubated at least 24 h before process. Confocal images were collected using ZEN software on an upright confocal microscope (LSM 710; Carl Zeiss; Plan Apochromatic 40×/1.3 Oil DIC M27 objective) with a color camera (DP-71 12 Mp) based on single confocal sections. The mCherry-TRAF2 puncta were detected as saturated pixels and counted above a background intensity threshold using minimum dark. 30 cells per condition were quantified using ImageJ software (The National Institutes of Health, Bethesda, MD, USA) and automatic particle counting above a threshold of 0.5 μm^2 in size.

H_2O_2 treatment

HeLa cells grown to 80% confluence were exposed to 1 mM or 3 mM H_2O_2 in DMEM supplemented with 10% FBS for 30 min at 37°C. After incubation, cells were in brief washed with ice-cold PBS three times and fixed using 4% PFA in PBS for 20 min, followed by additional washing step with PBS five times for 5 min.

Immunofluorescence imaging

Cells grown on coverslips were briefly washed with ice-cold PBS 3 times and fixed using 4% PFA in PBS for 20 min. After PBS washing two times for 5 min, cells were permeabilized using 0.1% Triton X-100 in PBS for 15 min and incubated with blocking buffer (5% BSA in PBS or TBST for anti-$CAV1^{Y14\text{-}p}$) overnight. Next day, the cells were washed with PBS or TBST (anti-$CAV1^{Y14\text{-}p}$), respectively, three times for 5 min and incubated with the appropriate primary and secondary (1:500) antibodies in 1% BSA in PBS or TBST (anti-$CAV1^{Y14\text{-}p}$), respectively, then mounted using Mowiol (Sigma-Aldrich). Confocal images were collected using ZEN software on an upright confocal microscope (LSM 710; Carl Zeiss; Plan Apochromatic 63×/1.40 Oil DIC M27 objective) with a color camera (DP-71 12 Mp).

Online supplemental material

Fig. S1 depicts immuno-EM of cf-caveolins. Fig. S2 depicts control experiments for the interaction screen. Fig. S3 depicts CAV1 interaction heat map analyzed by AlphaScreen. Fig. S4 depicts ABL kinases coexpression leads to the phosphorylation of $CAV1^{Y14}$. Fig. S5 depicts quantitative PLA detection for protein interactions.

Acknowledgments

The authors acknowledge the use of the Australian Microscopy & Microanalysis Research Facility at the Center for Microscopy and Microanalysis at The University of Queensland. We would also like to thank Alpha Yap, Brett Collins, Sergey Mureev, Tom Hall, Kerrie-Ann McMahon, Harriet Lo, and Susan Nixon for their input to the project.

This work was supported by grants and a fellowship from the National Health and Medical Research Council of Australia (grant numbers APP1037320, APP1058565, and APP569542 to R.G. Parton; APP1045092 to R.G. Parton and N. Ariotti; APP1100771 to Y. Gambin, E. Sierecki, and N. Ariotti) and from the Australian Research Council (Centre of Excellence in Convergent Bio-Nano Science and Technology and DP 150100505, R.G. Parton). Y. Gambin is supported by Australian Research Council Future Fellowship (grant FT110100478) and Discovery project (grant DP130102396).

The authors declare no competing financial interests.

Author contributions: R.G. Parton, N. Ariotti, Y. Gambin, and W. Jung designed experiments; W. Jung performed the biochemical experiments; W. Jung, C. Ferguson, R.G. Parton, and J. Rae performed the EM studies with assistance from N. Ariotti; Y. Gambin, E. Sierecki, and A. O'Carroll performed in vitro protein interaction analysis; K. Alexandrov designed the expression constructs and planned cf assays; W. Johnston and D.J.B. Hunter produced cf lysates; W. Jung and M. Bastiani performed the cell experiments; and R.G. Parton, N. Ariotti, Y. Gambin, and W. Jung wrote the manuscript.

Submitted: 3 July 2017
Revised: 24 January 2018
Accepted: 29 March 2018

References

Aboulaich, N., U. Ortegren, A.V. Vener, and P. Strålfors. 2006. Association and insulin regulated translocation of hormone-sensitive lipase with PTRF. *Biochem. Biophys. Res. Commun.* 350:657–661. https://doi.org/10.1016/j.bbrc.2006.09.094

Aoki, T., R. Nomura, and T. Fujimoto. 1999. Tyrosine phosphorylation of caveolin-1 in the endothelium. *Exp. Cell Res.* 253:629–636. https://doi.org/10.1006/excr.1999.4652

Ariotti, N., M.A. Fernández-Rojo, Y. Zhou, M.M. Hill, T.L. Rodkey, K.L. Inder, L.B. Tanner, M.R. Wenk, J.F. Hancock, and R.G. Parton. 2014. Caveolae regulate the nanoscale organization of the plasma membrane to remotely control Ras signaling. *J. Cell Biol.* 204:777–792. https://doi.org/10.1083/jcb.201307055

Ariotti, N., J. Rae, N. Leneva, C. Ferguson, D. Loo, S. Okano, M.M. Hill, P. Walser, B.M. Collins, and R.G. Parton. 2015. Molecular Characterization of Caveolin-induced Membrane Curvature. *J. Biol. Chem.* 290:24875–24890. https://doi.org/10.1074/jbc.M115.644336

Bernatchez, P.N., P.M. Bauer, J. Yu, J.S. Prendergast, P. He, and W.C. Sessa. 2005. Dissecting the molecular control of endothelial NO synthase by caveolin-1 using cell-permeable peptides. *Proc. Natl. Acad. Sci. USA.* 102:761–766. https://doi.org/10.1073/pnas.0407224102

Boettcher, J.P., M. Kirchner, Y. Churin, A. Kaushansky, M. Pompaiah, H. Thorn, V. Brinkmann, G. Macbeath, and T.F. Meyer. 2010.

Tyrosine-phosphorylated caveolin-1 blocks bacterial uptake by inducing Vav2-RhoA-mediated cytoskeletal rearrangements. *PLoS Biol.* 8:e1000457. https://doi.org/10.1371/journal.pbio.1000457

Boucrot, E., M.T. Howes, T. Kirchhausen, and R.G. Parton. 2011. Redistribution of caveolae during mitosis. *J. Cell Sci.* 124:1965–1972. https://doi.org/10.1242/jcs.076570

Breen, M.R., M. Camps, F. Carvalho-Simoes, A. Zorzano, and P.F. Pilch. 2012. Cholesterol depletion in adipocytes causes caveolae collapse concomitant with proteosomal degradation of cavin-2 in a switch-like fashion. *PLoS One.* 7:e34516. https://doi.org/10.1371/journal.pone.0034516

Brennan, D., S. Peltonen, A. Dowling, W. Medhat, K.J. Green, J.K. Wahl III, F. Del Galdo, and M.G. Mahoney. 2012. A role for caveolin-1 in desmoglein binding and desmosome dynamics. *Oncogene.* 31:1636–1648. https://doi.org/10.1038/onc.2011.346

Burgermeister, E., T. Friedrich, I. Hitkova, I. Regel, H. Einwächter, W. Zimmermann, C. Röcken, A. Perren, M.B. Wright, R.M. Schmid, et al. 2011. The Ras inhibitors caveolin-1 and docking protein 1 activate peroxisome proliferator-activated receptor γ through spatial relocalization at helix 7 of its ligand-binding domain. *Mol. Cell. Biol.* 31:3497–3510. https://doi.org/10.1128/MCB.01421-10

Byrne, D.P., C. Dart, and D.J. Rigden. 2012. Evaluating caveolin interactions: do proteins interact with the caveolin scaffolding domain through a widespread aromatic residue-rich motif? *PLoS One.* 7:e44879. https://doi.org/10.1371/journal.pone.0044879

Cao, H., W.E. Courchesne, and C.C. Mastick. 2002. A phosphotyrosine-dependent protein interaction screen reveals a role for phosphorylation of caveolin-1 on tyrosine 14: recruitment of C-terminal Src kinase. *J. Biol. Chem.* 277:8771–8774. https://doi.org/10.1074/jbc.C100661200

Caselli, A., B. Mazzinghi, G. Camici, G. Manao, and G. Ramponi. 2002. Some protein tyrosine phosphatases target in part to lipid rafts and interact with caveolin-1. *Biochem. Biophys. Res. Commun.* 296:692–697. https://doi.org/10.1016/S0006-291X(02)00928-2

Chaudhary, N., G.A. Gomez, M.T. Howes, H.P. Lo, K.A. McMahon, J.A. Rae, N.L. Schieber, M.M. Hill, K. Gaus, A.S. Yap, and R.G. Parton. 2014. Endocytic crosstalk: cavins, caveolins, and caveolae regulate clathrin-independent endocytosis. *PLoS Biol.* 12:e1001832. https://doi.org/10.1371/journal.pbio.1001832

Chen, D.B., S.M. Li, X.X. Qian, C. Moon, and J. Zheng. 2005. Tyrosine phosphorylation of caveolin 1 by oxidative stress is reversible and dependent on the c-src tyrosine kinase but not mitogen-activated protein kinase pathways in placental artery endothelial cells. *Biol. Reprod.* 73:761–772. https://doi.org/10.1095/biolreprod.105.040881

Collins, B.M., M.J. Davis, J.F. Hancock, and R.G. Parton. 2012. Structure-based reassessment of the caveolin signaling model: do caveolae regulate signaling through caveolin-protein interactions? *Dev. Cell.* 23:11–20. https://doi.org/10.1016/j.devcel.2012.06.012

Couet, J., S. Li, T. Okamoto, T. Ikezu, and M.P. Lisanti. 1997a. Identification of peptide and protein ligands for the caveolin-scaffolding domain. Implications for the interaction of caveolin with caveolae-associated proteins. *J. Biol. Chem.* 272:6525–6533. https://doi.org/10.1074/jbc.272.10.6525

Couet, J., L. Shengwen, T. Okamoto, P.E. Scherer, and M.P. Lisanti. 1997b. Molecular and cellular biology of caveolae paradoxes and plasticities. *Trends Cardiovasc. Med.* 7:103–110. https://doi.org/10.1016/S1050-1738(97)00001-7

del Pozo, M.A., N. Balasubramanian, N.B. Alderson, W.B. Kiosses, A. Grande-García, R.G. Anderson, and M.A. Schwartz. 2005. Phospho-caveolin-1 mediates integrin-regulated membrane domain internalization. *Nat. Cell Biol.* 7:901–908. https://doi.org/10.1038/ncb1293

Drab, M., P. Verkade, M. Elger, M. Kasper, M. Lohn, B. Lauterbach, J. Menne, C. Lindschau, F. Mende, F.C. Luft, et al. 2001. Loss of caveolae, vascular dysfunction, and pulmonary defects in caveolin-1 gene-disrupted mice. *Science.* 293:2449–2452. https://doi.org/10.1126/science.1062688

Feng, X., M.L. Gaeta, L.A. Madge, J.H. Yang, J.R. Bradley, and J.S. Pober. 2001. Caveolin-1 associates with TRAF2 to form a complex that is recruited to tumor necrosis factor receptors. *J. Biol. Chem.* 276:8341–8349. https://doi.org/10.1074/jbc.M007116200

Feron, O., L. Belhassen, L. Kobzik, T.W. Smith, R.A. Kelly, and T. Michel. 1996. Endothelial nitric oxide synthase targeting to caveolae. Specific interactions with caveolin isoforms in cardiac myocytes and endothelial cells. *J. Biol. Chem.* 271:22810–22814. https://doi.org/10.1074/jbc.271.37.22810

Fielding, P.E., P. Chau, D. Liu, T.A. Spencer, and C.J. Fielding. 2004. Mechanism of platelet-derived growth factor-dependent caveolin-1 phosphorylation: relationship to sterol binding and the role of serine-80. *Biochemistry.* 43:2578–2586. https://doi.org/10.1021/bi035442c

García-Cardeña, G., P. Oh, J. Liu, J.E. Schnitzer, and W.C. Sessa. 1996. Targeting of nitric oxide synthase to endothelial cell caveolae via palmitoylation: implications for nitric oxide signaling. *Proc. Natl. Acad. Sci. USA.* 93:6448–6453. https://doi.org/10.1073/pnas.93.13.6448

García-Cardeña, G., P. Martasek, B.S. Masters, P.M. Skidd, J. Couet, S. Li, M.P. Lisanti, and W.C. Sessa. 1997. Dissecting the interaction between nitric oxide synthase (NOS) and caveolin. Functional significance of the nos caveolin binding domain in vivo. *J. Biol. Chem.* 272:25437–25440. https://doi.org/10.1074/jbc.272.41.25437

Gingras, D., F. Gauthier, S. Lamy, R.R. Desrosiers, and R. Béliveau. 1998. Localization of RhoA GTPase to endothelial caveolae-enriched membrane domains. *Biochem. Biophys. Res. Commun.* 247:888–893. https://doi.org/10.1006/bbrc.1998.8885

Glenney, J.R. Jr., and L. Zokas. 1989. Novel tyrosine kinase substrates from Rous sarcoma virus-transformed cells are present in the membrane skeleton. *J. Cell Biol.* 108:2401–2408. https://doi.org/10.1083/jcb.108.6.2401

Gratton, J.P., M.I. Lin, J. Yu, E.D. Weiss, Z.L. Jiang, T.A. Fairchild, Y. Iwakiri, R. Groszmann, K.P. Claffey, Y.C. Cheng, and W.C. Sessa. 2003. Selective inhibition of tumor microvascular permeability by cavtratin blocks tumor progression in mice. *Cancer Cell.* 4:31–39. https://doi.org/10.1016/S1535-6108(03)00168-5

Gustincich, S., P. Vatta, S. Goruppi, M. Wolf, S. Saccone, G. Della Valle, M. Baggiolini, and C. Schneider. 1999. The human serum deprivation response gene (SDPR) maps to 2q32-q33 and codes for a phosphatidylserine-binding protein. *Genomics.* 57:120–129. https://doi.org/10.1006/geno.1998.5733

Hailstones, D., L.S. Sleer, R.G. Parton, and K.K. Stanley. 1998. Regulation of caveolin and caveolae by cholesterol in MDCK cells. *J. Lipid Res.* 39:369–379.

Hansen, C.G., and B.J. Nichols. 2010. Exploring the caves: cavins, caveolins and caveolae. *Trends Cell Biol.* 20:177–186. https://doi.org/10.1016/j.tcb.2010.01.005

Hayer, A., M. Stoeber, C. Bissig, and A. Helenius. 2010. Biogenesis of caveolae: stepwise assembly of large caveolin and cavin complexes. *Traffic.* 11:361–382. https://doi.org/10.1111/j.1600-0854.2009.01023.x

Hill, M.M., M. Bastiani, R. Luetterforst, M. Kirkham, A. Kirkham, S.J. Nixon, P. Walser, D. Abankwa, V.M. Oorschot, S. Martin, et al. 2008. PTRF-Cavin, a conserved cytoplasmic protein required for caveola formation and function. *Cell.* 132:113–124. https://doi.org/10.1016/j.cell.2007.11.042

Hirama, T., R. Das, Y. Yang, C. Ferguson, A. Won, C.M. Yip, J.G. Kay, S. Grinstein, R.G. Parton, and G.D. Fairn. 2017. Phosphatidylserine dictates the assembly and dynamics of caveolae in the plasma membrane. *J. Biol. Chem.* 292:14292–14307. https://doi.org/10.1074/jbc.M117.791400

Hoffmann, C., A. Berking, F. Agerer, A. Buntru, F. Neske, G.S. Chhatwal, K. Ohlsen, and C.R. Hauck. 2010. Caveolin limits membrane microdomain mobility and integrin-mediated uptake of fibronectin-binding pathogens. *J. Cell Sci.* 123:4280–4291. https://doi.org/10.1242/jcs.064006

Hupalowska, A., B. Pyrzynska, and M. Miaczynska. 2012. APPL1 regulates basal NF-kappaB activity by stabilizing NIK. *J. Cell Sci.* 125:4090–4102. https://doi.org/10.1242/jcs.105171

Joshi, B., M. Bastiani, S.S. Strugnell, C. Boscher, R.G. Parton, and I.R. Nabi. 2012. Phosphocaveolin-1 is a mechanotransducer that induces caveola biogenesis via Egr1 transcriptional regulation. *J. Cell Biol.* 199:425–435. https://doi.org/10.1083/jcb.201207089

Ju, H., R. Zou, V.J. Venema, and R.C. Venema. 1997. Direct interaction of endothelial nitric-oxide synthase and caveolin-1 inhibits synthase activity. *J. Biol. Chem.* 272:18522–18525. https://doi.org/10.1074/jbc.272.30.18522

Karpen, H.E., J.T. Bukowski, T. Hughes, J.P. Gratton, W.C. Sessa, and M.R. Gailani. 2001. The sonic hedgehog receptor patched associates with caveolin-1 in cholesterol-rich microdomains of the plasma membrane. *J. Biol. Chem.* 276:19503–19511. https://doi.org/10.1074/jbc.M010832200

Kirkham, M., S.J. Nixon, M.T. Howes, L. Abi-Rached, D.E. Wakeham, M. Hanzal-Bayer, C. Ferguson, M.M. Hill, M. Fernandez-Rojo, D.A. Brown, et al. 2008. Evolutionary analysis and molecular dissection of caveola biogenesis. *J. Cell Sci.* 121:2075–2086. https://doi.org/10.1242/jcs.024588

Kovtun, O., S. Mureev, W. Jung, M.H. Kubala, W. Johnston, and K. Alexandrov. 2011. Leishmania cell-free protein expression system. *Methods.* 55:58–64. https://doi.org/10.1016/j.ymeth.2011.06.006

Kovtun, O., V.A. Tillu, N. Ariotti, R.G. Parton, and B.M. Collins. 2015. Cavin family proteins and the assembly of caveolae. *J. Cell Sci.* 128:1269–1278. https://doi.org/10.1242/jcs.167866

Lee, H., D. Volonte, F. Galbiati, P. Iyengar, D.M. Lublin, D.B. Bregman, M.T. Wilson, R. Campos-Gonzalez, B. Bouzahzah, R.G. Pestell, et al. 2000.

Constitutive and growth factor-regulated phosphorylation of caveolin-1 occurs at the same site (Tyr-14) in vivo: identification of a c-Src/Cav-1/Grb7 signaling cassette. *Mol. Endocrinol.* 14:1750–1775. https://doi.org/10.1210/mend.14.11.0553

Li, H., and V. Papadopoulos. 1998. Peripheral-type benzodiazepine receptor function in cholesterol transport. Identification of a putative cholesterol recognition/interaction amino acid sequence and consensus pattern. *Endocrinology.* 139:4991–4997. https://doi.org/10.1210/endo.139.12.6390

Li, S., T. Okamoto, M. Chun, M. Sargiacomo, J.E. Casanova, S.H. Hansen, I. Nishimoto, and M.P. Lisanti. 1995. Evidence for a regulated interaction between heterotrimeric G proteins and caveolin. *J. Biol. Chem.* 270:15693–15701. https://doi.org/10.1074/jbc.270.26.15693

Li, S., J. Couet, and M.P. Lisanti. 1996a. Src tyrosine kinases, Galpha subunits, and H-Ras share a common membrane-anchored scaffolding protein, caveolin. *J. Biol. Chem.* 271:29182–29190. https://doi.org/10.1074/jbc.271.46.29182

Li, S., R. Seitz, and M.P. Lisanti. 1996b. Phosphorylation of caveolin by src tyrosine kinases. The alpha-isoform of caveolin is selectively phosphorylated by v-Src in vivo. *J. Biol. Chem.* 271:3863–3868. https://doi.org/10.1074/jbc.271.7.3863

Lingappa, V.R., J.R. Lingappa, R. Prasad, K.E. Ebner, and G. Blobel. 1978. Coupled cell-free synthesis, segregation, and core glycosylation of a secretory protein. *Proc. Natl. Acad. Sci. USA.* 75:2338–2342. https://doi.org/10.1073/pnas.75.5.2338

Lisanti, M.P., Z. Tang, P.E. Scherer, E. Kübler, A.J. Koleske, and M. Sargiacomo. 1995. Caveolae, transmembrane signalling and cellular transformation. *Mol. Membr. Biol.* 12:121–124. https://doi.org/10.3109/09687689509038506

Liu, P., M. Rudick, and R.G. Anderson. 2002. Multiple functions of caveolin-1. *J. Biol. Chem.* 277:41295–41298. https://doi.org/10.1074/jbc.R200020200

Mastick, C.C., M.J. Brady, and A.R. Saltiel. 1995. Insulin stimulates the tyrosine phosphorylation of caveolin. *J. Cell Biol.* 129:1523–1531. https://doi.org/10.1083/jcb.129.6.1523

Mastick, C.C., A.R. Sanguinetti, J.H. Knesek, G.S. Mastick, and L.F. Newcomb. 2001. Caveolin-1 and a 29-kDa caveolin-associated protein are phosphorylated on tyrosine in cells expressing a temperature-sensitive v-Abl kinase. *Exp. Cell Res.* 266:142–154. https://doi.org/10.1006/excr.2001.5205

Michel, J.B., O. Feron, K. Sase, P. Prabhakar, and T. Michel. 1997. Caveolin versus calmodulin. *J. Biol. Chem.* 272:25907–25912. https://doi.org/10.1074/jbc.272.41.25907

Mineo, C., Y.S. Ying, C. Chapline, S. Jaken, and R.G. Anderson. 1998. Targeting of protein kinase Calpha to caveolae. *J. Cell Biol.* 141:601–610. https://doi.org/10.1083/jcb.141.3.601

Mo, S., L. Wang, Q. Li, J. Li, Y. Li, V.J. Thannickal, and Z. Cui. 2010. Caveolin-1 regulates dorsoventral patterning through direct interaction with beta-catenin in zebrafish. *Dev. Biol.* 344:210–223. https://doi.org/10.1016/j.ydbio.2010.04.033

Morén, B., C. Shah, M.T. Howes, Schieber N.L., H.T. McMahon, R.G. Parton, O. Daumke, and R. Lundmark. 2012. EHD2 regulates caveolar dynamics via ATP-driven targeting and oligomerization. *Molecular Biology of the Cell.* 23:1316–1329. https://doi.org/10.1091/mbc.E11-09-0787

Mureev, S., O. Kovtun, U.T. Nguyen, and K. Alexandrov. 2009. Species-independent translational leaders facilitate cell-free expression. *Nat. Biotechnol.* 27:747–752. https://doi.org/10.1038/nbt.1556

Okamoto, T., A. Schlegel, P.E. Scherer, and M.P. Lisanti. 1998. Caveolins, a family of scaffolding proteins for organizing "preassembled signaling complexes" at the plasma membrane. *J. Biol. Chem.* 273:5419–5422. https://doi.org/10.1074/jbc.273.10.5419

Park, D.S., H. Lee, P.G. Frank, B. Razani, A.V. Nguyen, A.F. Parlow, R.G. Russell, J. Hulit, R.G. Pestell, and M.P. Lisanti. 2002. Caveolin-1-deficient mice show accelerated mammary gland development during pregnancy, premature lactation, and hyperactivation of the Jak-2/STAT5a signaling cascade. *Mol. Biol. Cell.* 13:3416–3430. https://doi.org/10.1091/mbc.02-05-0071

Park, H., K.J. Ahn, J. Lee Kang, and Y.H. Choi. 2015. Protein-protein interaction between caveolin-1 and SHP-2 is dependent on the N-SH2 domain of SHP-2. *BMB Rep.* 48:184–189. https://doi.org/10.5483/BMBRep.2015.48.3.249

Parton, R.G., and M.A. del Pozo. 2013. Caveolae as plasma membrane sensors, protectors and organizers. *Nat. Rev. Mol. Cell Biol.* 14:98–112. https://doi.org/10.1038/nrm3512

Parton, R.G., and K. Simons. 2007. The multiple faces of caveolae. *Nat. Rev. Mol. Cell Biol.* 8:185–194. https://doi.org/10.1038/nrm2122

Pelkmans, L., and M. Zerial. 2005. Kinase-regulated quantal assemblies and kiss-and-run recycling of caveolae. *Nature.* 436:128–133. https://doi.org/10.1038/nature03866

Pelkmans, L., T. Bürli, M. Zerial, and A. Helenius. 2004. Caveolin-stabilized membrane domains as multifunctional transport and sorting devices in endocytic membrane traffic. *Cell.* 118:767–780. https://doi.org/10.1016/j.cell.2004.09.003

Pike, L.J. 2005. Growth factor receptors, lipid rafts and caveolae: an evolving story. *Biochim. Biophys. Acta.* 1746:260–273. https://doi.org/10.1016/j.bbamcr.2005.05.005

Radel, C., and V. Rizzo. 2005. Integrin mechanotransduction stimulates caveolin-1 phosphorylation and recruitment of Csk to mediate actin reorganization. *Am. J. Physiol. Heart Circ. Physiol.* 288:H936–H945. https://doi.org/10.1152/ajpheart.00519.2004

Razani, B., J.A. Engelman, X.B. Wang, W. Schubert, X.L. Zhang, C.B. Marks, F. Macaluso, R.G. Russell, M. Li, R.G. Pestell, et al. 2001. Caveolin-1 null mice are viable but show evidence of hyperproliferative and vascular abnormalities. *J. Biol. Chem.* 276:38121–38138.

Rothberg, K.G., J.E. Heuser, W.C. Donzell, Y.S. Ying, J.R. Glenney, and R.G. Anderson. 1992. Caveolin, a protein component of caveolae membrane coats. *Cell.* 68:673–682. https://doi.org/10.1016/0092-8674(92)90143-Z

Rothman, J.E. 1988. Reconstruction of organelle function in cell-free systems: introduction. *Prog. Clin. Biol. Res.* 270:311–316.

Sanguinetti, A.R., and C.C. Mastick. 2003. c-Abl is required for oxidative stress-induced phosphorylation of caveolin-1 on tyrosine 14. *Cell. Signal.* 15:289–298. https://doi.org/10.1016/S0898-6568(02)00090-6

Sato, Y., I. Sagami, and T. Shimizu. 2004. Identification of caveolin-1-interacting sites in neuronal nitric-oxide synthase. Molecular mechanism for inhibition of NO formation. *J. Biol. Chem.* 279:8827–8836. https://doi.org/10.1074/jbc.M310327200

Scheel, J., J. Srinivasan, U. Honnert, A. Henske, and T.V. Kurzchalia. 1999. Involvement of caveolin-1 in meiotic cell-cycle progression in Caenorhabditis elegans. *Nat. Cell Biol.* 1:127–129. https://doi.org/10.1038/10100

Scherer, P.E., M.P. Lisanti, G. Baldini, M. Sargiacomo, C.C. Mastick, and H.F. Lodish. 1994. Induction of caveolin during adipogenesis and association of GLUT4 with caveolin-rich vesicles. *J. Cell Biol.* 127:1233–1243. https://doi.org/10.1083/jcb.127.5.1233

Schlegel, A., R.B. Schwab, P.E. Scherer, and M.P. Lisanti. 1999. A role for the caveolin scaffolding domain in mediating the membrane attachment of caveolin-1. The caveolin scaffolding domain is both necessary and sufficient for membrane binding in vitro. *J. Biol. Chem.* 274:22660–22667. https://doi.org/10.1074/jbc.274.32.22660

Schou, K.B., J.B. Mogensen, S.K. Morthorst, B.S. Nielsen, A. Aleliunaite, A. Serra-Marques, N. Fürstenberg, S. Saunier, A.A. Bizet, I.R. Veland, et al. 2017. KIF13B establishes a CAV1-enriched microdomain at the ciliary transition zone to promote Sonic hedgehog signalling. *Nat. Commun.* 8:14177. https://doi.org/10.1038/ncomms14177

Senju, Y., Y. Itoh, K. Takano, S. Hamada, and S. Suetsugu. 2011. Essential role of PACSIN2/syndapin-II in caveolae membrane sculpting. *J. Cell Sci.* 124:2032–2040. https://doi.org/10.1242/jcs.086264

Shajahan, A.N., Z.C. Dobbin, F.E. Hickman, S. Dakshanamurthy, and R. Clarke. 2012. Tyrosine-phosphorylated caveolin-1 (Tyr-14) increases sensitivity to paclitaxel by inhibiting BCL2 and BCLxL proteins via c-Jun N-terminal kinase (JNK). *J. Biol. Chem.* 287:17682–17692. https://doi.org/10.1074/jbc.M111.304022

Shen, H.M., Y. Lin, S. Choksi, J. Tran, T. Jin, L. Chang, M. Karin, J. Zhang, and Z.G. Liu. 2004. Essential roles of receptor-interacting protein and TRAF2 in oxidative stress-induced cell death. *Mol. Cell. Biol.* 24:5914–5922. https://doi.org/10.1128/MCB.24.13.5914-5922.2004

Sierecki, E., L.M. Stevers, N. Giles, M.E. Polinkovsky, M. Moustaqil, S. Mureev, W.A. Johnston, M. Dahmer-Heath, D. Skalamera, T.J. Gonda, et al. 2014. Rapid mapping of interactions between Human SNX-BAR proteins measured in vitro by AlphaScreen and single-molecule spectroscopy. *Mol. Cell. Proteomics.* 13:2233–2245. https://doi.org/10.1074/mcp.M113.037275

Song, K.S., T. Li Shengwen, T. Okamoto, L.A. Quilliam, M. Sargiacomo, and M.P. Lisanti. 1996. Co-purification and direct interaction of Ras with caveolin, an integral membrane protein of caveolae microdomains. Detergent-free purification of caveolae microdomains. *J. Biol. Chem.* 271:9690–9697. https://doi.org/10.1074/jbc.271.16.9690

Song, K.S., M. Sargiacomo, F. Galbiati, M. Parenti, and M.P. Lisanti. 1997. Targeting of a G alpha subunit (Gi1 alpha) and c-Src tyrosine kinase to caveolae membranes: clarifying the role of N-myristoylation. *Cell. Mol. Biol.* 43:293–303.

Songyang, Z., and L.C. Cantley. 1995. Recognition and specificity in protein tyrosine kinase-mediated signalling. *Trends Biochem. Sci.* 20:470–475. https://doi.org/10.1016/S0968-0004(00)89103-3

Subach, O.M., I.S. Gundorov, M. Yoshimura, F.V. Subach, J. Zhang, D. Grüenwald, E.A. Souslova, D.M. Chudakov, and V.V. Verkhusha. 2008. Conversion of red fluorescent protein into a bright blue probe. *Chem. Biol.* 15:1116–1124. https://doi.org/10.1016/j.chembiol.2008.08.006

Sun, X.H., D.C. Flynn, V. Castranova, L.L. Millecchia, A.R. Beardsley, and J. Liu. 2007. Identification of a novel domain at the N terminus of caveolin-1 that controls rear polarization of the protein and caveolae formation. *J. Biol. Chem.* 282:7232–7241. https://doi.org/10.1074/jbc.M607396200

Tran, J., A. Magenau, M. Rodriguez, C. Rentero, T. Royo, C. Enrich, S.R. Thomas, T. Grewal, and K. Gaus. 2016. Activation of Endothelial Nitric Oxide (eNOS) Occurs through Different Membrane Domains in Endothelial Cells. *PLoS One.* 11:e0151556. https://doi.org/10.1371/journal.pone.0151556

Volonté, D., F. Galbiati, R.G. Pestell, and M.P. Lisanti. 2001. Cellular stress induces the tyrosine phosphorylation of caveolin-1 (Tyr(14)) via activation of p38 mitogen-activated protein kinase and c-Src kinase. Evidence for caveolae, the actin cytoskeleton, and focal adhesions as mechanical sensors of osmotic stress. *J. Biol. Chem.* 276:8094–8103. https://doi.org/10.1074/jbc.M009245200

Walser, P.J., N. Ariotti, M. Howes, C. Ferguson, R. Webb, D. Schwudke, N. Leneva, K.J. Cho, L. Cooper, J. Rae, et al. 2012. Constitutive formation of caveolae in a bacterium. *Cell.* 150:752–763. https://doi.org/10.1016/j.cell.2012.06.042

Wang, Y., X. Wang, J.F. Jasmin, W.B. Lau, R. Li, Y. Yuan, W. Yi, K. Chuprun, M.P. Lisanti, W.J. Koch, et al. 2012. Essential role of caveolin-3 in adiponectin signalsome formation and adiponectin cardioprotection. *Arterioscler. Thromb. Vasc. Biol.* 32:934–942. https://doi.org/10.1161/ATVBAHA.111.242164

Wary, K.K., A. Mariotti, C. Zurzolo, and F.G. Giancotti. 1998. A requirement for caveolin-1 and associated kinase Fyn in integrin signaling and anchorage-dependent cell growth. *Cell.* 94:625–634. https://doi.org/10.1016/S0092-8674(00)81604-9

Xia, H., W. Khalil, J. Kahm, J. Jessurun, J. Kleidon, and C.A. Henke. 2010. Pathologic caveolin-1 regulation of PTEN in idiopathic pulmonary fibrosis. *Am. J. Pathol.* 176:2626–2637. https://doi.org/10.2353/ajpath.2010.091117

Yao, Q., J. Chen, H. Cao, J.D. Orth, J.M. McCaffery, R.V. Stan, and M.A. McNiven. 2005. Caveolin-1 interacts directly with dynamin-2. *J. Mol. Biol.* 348:491–501. https://doi.org/10.1016/j.jmb.2005.02.003

Zhang, B., F. Peng, D. Wu, A.J. Ingram, B. Gao, and J.C. Krepinsky. 2007. Caveolin-1 phosphorylation is required for stretch-induced EGFR and Akt activation in mesangial cells. *Cell. Signal.* 19:1690–1700. https://doi.org/10.1016/j.cellsig.2007.03.005

Zimnicka, A., Y. Husain, A. Shajahan, P. Toth, and R. Minshall. 2015. Phosphorylation of Caveolin-1 Tyrosine 14 Leads to Caveolar Coat Destabilization, Membrane Invagination and Endocytosis. *FASEB J.* 29.